BAYESIAN ESTIMATION OF COVARIATE ASSISTED PRINCIPAL REGRESSION FOR BRAIN FUNCTIONAL CONNECTIVITY

A PREPRINT

Hyung G. Park
Division of Biostatistics, Department of Population Health
New York University School of Medicine
New York, NY 10016
parkh15@nyu.edu

ABSTRACT

This paper presents a Bayesian reformulation of covariate-assisted principal (CAP) regression of Zhao et al. [2021a], which aims to identify components in the covariance of response signal that are associated with covariates in a regression framework. We introduce a geometric formulation and reparameterization of individual covariance matrices in their tangent space. By mapping the covariance matrices to the tangent space, we leverage Euclidean geometry to perform posterior inference. This approach enables joint estimation of all parameters and uncertainty quantification within a unified framework, fusing dimension reduction for covariance matrices with regression model estimation. We validate the proposed method through simulation studies and apply it to analyze associations between covariates and brain functional connectivity, utilizing data from the Human Connectome Project.

Keywords Dimension reduction · Heteroscedasticity · Brain functional connectivity

1 Introduction

This paper reformulates covariate-assisted principal (CAP) regression of Zhao et al. [2021a] in the Bayesian paradigm. The approach identifies covariate-relevant components of the covariance of multivariate response data. Specifically, the method estimates a set of linear projections of multivariate response signals, whose variance is related with covariates. In neuroscience, there is interest in analyzing statistical dependency between time-series of brain signals in distinct regions of the brain, which we refer to as functional connectivity (FC) [Fox and Dunson, 2015, Lindquist, 2008, Monti et al., 2014, Fornito et al., 2013, Fornito and Bullmore, 2012], as this statistical dependency is related with behavioral characteristics. The brain signals that underlie FC are multivariate, and each brain activity is considered relative to others [Varoquaux et al., 2010] in analyzing FC. This paper develops a Bayesian approach that simultaneously conducts dimension reduction of the multivariate signals to analyze the association between covariates and the FC characterized by the covariance between the brain signals.

Typically, the first step to analyze brain FC is to define a set of nodes corresponding to spatial regions of interest (ROIs), where each node is associated with its own time course of imaging data. Then the network connections (or an "edge" structure between the nodes) are subsequently estimated based on the statistical dependency between each of the nodes' time course [Friston, 2011, van der Heuvel and Hulshoff Pol, 2010]. FC networks have been inferred using Pearson's correlation coefficients [Hutchison et al., 2013] and also with partial correlations in the context of Gaussian graphical models [Whittaker, 1990, Hinne et al., 2014] summarized in the precision or inverse covariance matrix. In recent years, there has been a focus on subject-level graphical models where the node-to-node dependencies vary with respect to subject-level covariates. This line of research involves methods to estimate or test group-specific graphs [Guo et al., 2011, Danaher et al., 2014, Xia and Li, 2017, Xia et al., 2018, Narayan et al., 2015, Durante and Dunson, 2018, Xia et al., 2015, Cai et al., 2016, Saegusa and Shojaie, 2016, Peterson et al., 2015, Tan et al., 2017, Lin et al., 2017] as well as general Gaussian graphical models for graph edges that allow both continuous and discrete covariates, estimated based on trees [Liu et al., 2010], kernels [Kolar et al., 2010, Lee and Xue, 2018], linear or additive regression [Ni et al.,

2019, Wang et al., 2022, Zhang and Li, 2022]. However, like other standard node-wise regression methods [e.g., Leday et al., 2017, Meinshausen and Buhlmann, 2006, Peng et al., 2009, Kolar et al., 2010, Cheng et al., 2014, Ha et al., 2021] in graphical models, these approaches focus on edge detection (i.e., estimation of the off-diagonal elements) rather than estimating the full precision or covariance matrix and do not explicitly constrain positive definiteness of precision or covariance matrices. Works on general tensor outcome regression [Sun and Li, 2017, Li and Zhang, 2017, Lock, 2018] also do not generally guarantee the positive definiteness of the outcomes. While the problem of dimension reduction of individual covariances has been studied in brain dynamic connectivity analysis [Dai et al., 2020], problems in computer vision [Harandi et al., 2017, Li and Lu, 2018, Gao et al., 2023] and brain computer interfaces [Xie et al., 2017, Davoudi et al., 2017] as well as multi-group covariance estimation [Flury, 1984, 1986, Boik, 2002, Pourahmadi et al., 2007, Hoff, 2009, Franks and Hoff, 2019], covariate information was not utilized in conducting dimension reduction. Gaussian graphical models have been applied to study brain connectivity networks in fMRI data [e.g., Li and Solea, 2018, Zhang et al., 2020], however, the focus was on analyzing connectivity networks without explicitly considering their relationship with subject-level covariates.

In this paper, in line with the covariance regression literatures [see, e.g., Hoff and Niu, 2012, Fox and Dunson, 2015, Zou et al., 2017, Pourahmadi, 2011, Varoquaux et al., 2010, Zhao et al., 2021a,b, 2022, Engle and Kroner, 1995, Fong et al., 2006], we will frame the problem of analyzing FC as modeling of heteroscedasticity, i.e., estimating a covariance function $\boldsymbol{\Sigma}_{\boldsymbol{x}} = \text{var}[\boldsymbol{Y}|\boldsymbol{x}]$ across a range of values for an explanatory $\boldsymbol{x}$-variable. Specifically, we consider a generalized linear model of the form $g(\boldsymbol{\Sigma}_i) = \boldsymbol{x}_i^\top \boldsymbol{\beta}$ for covariance, where $g(\cdot)$ is a link function (that incorporates unknown dimension reduction components) to relate a $p \times p$ symmetric positive definite (SPD) matrix to a linear predictor. In contrast to the approach developed in Zhao et al. [2021a] where each dimension-reduction vector for $\boldsymbol{\Sigma}_i$ is estimated sequentially or separately, the proposed framework allows coherent and simultaneous inference on all model parameters within the Bayesian paradigm.

The outcome data of interest are multivariate time-series resting-state fMRI (rs-fMRI) data in $\mathbb{R}^p$ measured simultaneously across the p ROIs (or parcels) defined based on an anatomical parcellation [Eickhoff et al., 2018] or "network nodes" [Smith et al., 2012] derived based on a data-driven algorithm, such as independent component analysis (ICA) [Calhoun et al., 2009, Smith et al., 2013]. We will apply the proposed Bayesian CAP regression to data from the Human Connectome Project (HCP) [Van Essen et al., 2013] to compare short sleepers (i.e., $\leq$ 6 hours) with conventional sleepers (i.e., 7 to 9 hours) with respect to their FC, as in Seiler and Holmes [2017].

One typical approach to associating brain FC with behavior is to take a massive univariate test approach that relates each connectivity matrix element with subject-level covariates [e.g., Grillon et al., 2013, Woodward et al., 2011]. However, this "massive edgewise regression" lacks statistical power, as it (i) ignores dependencies among the connectivity matrix elements; and (ii) involves quadratically increasing number of regressions that exacerbate the problem of multiple testing. On the other hand, multivariate methods, such as principal component analysis (PCA), consider the data from all ROIs at once which is useful if we believe that multiple brain regions work together to accomplish cognitive tasks [Seiler and Holmes, 2017], and can reduce the dimensionality of the original outcome to a smaller number of "networks" components.

In this paper, instead of directly modeling the subject-level covariance matrices $\boldsymbol{\Sigma}_i$ (as in Seiler and Holmes [2017], Fox and Dunson [2015], Zou et al. [2017]) where most of the node-wise connections' heterogeneity may be unrelated with covariates $\boldsymbol{x}_i$, we estimate a lower dimensional component within $\boldsymbol{\Sigma}_i$ associated with $\boldsymbol{x}_i$. We will characterize this lower dimensional structure by an orthonormal matrix $\boldsymbol{\Gamma} \in \mathbb{R}^{p\times d}$ where $\boldsymbol{\Gamma}^\top\boldsymbol{\Gamma} = \boldsymbol{I}_d$ (i.e., $\boldsymbol{\Gamma}$ is in a Stiefel manifold) with $d \leq p$.

For a multivariate outcome signal $\boldsymbol{Y}_{i,l} \in \mathbb{R}^p$ at volume (i.e., time point) l for subject i, Seiler and Holmes [2017] utilized the following heteroscedesticity model

$$\text{var}(\boldsymbol{Y}_{i,l}) = \boldsymbol{B}\boldsymbol{x}_i\boldsymbol{x}_i^\top\boldsymbol{B}^\top + \sigma^2\boldsymbol{I}_p \quad (l = 1, \ldots, T_i)(i = 1, \ldots, n), \tag{1}$$

where the covariance matrix $\boldsymbol{\Sigma}_i = \text{var}(\boldsymbol{Y}_{i,l})$ of the outcome is a quadratic function of $\boldsymbol{B}\boldsymbol{x}_i \in \mathbb{R}^p$ with covariates $\boldsymbol{x}_i \in \mathbb{R}^q$, and $\boldsymbol{B} \in \mathbb{R}^{p\times q}$ and $\sigma^2 > 0$ are unknown parameters. Model (1) is quite restrictive since the noise covariance $\sigma^2\boldsymbol{I}_p$ is diagonal with independent variances. On the other hand, the general version proposed by Hoff and Niu [2012] replaces $\sigma^2\boldsymbol{I}_p$ by a $p \times p$ SPD matrix, requiring a large number of parameters (that can scale quadratically in p). The approaches proposed in Fox and Dunson [2015], Zou et al. [2017] also similarly model the whole $p \times p$ matrix $\text{var}(\boldsymbol{Y}_{i,l})$ as outcomes, which may make the interpretation challenging for large matrices [Zhao et al., 2021a].

Zhao et al. [2021a] considered

$$\log \text{var}(\boldsymbol{\gamma}^{(k)\top}\boldsymbol{Y}_{i,l}) = \boldsymbol{x}_i^\top\boldsymbol{\beta}^{(k)} \tag{2}$$

where the directions for outcome projection $\boldsymbol{\gamma}^{(k)}$ $(k = 1, \ldots, d)$ are sequentially estimated, subject to identifiability constraints $\boldsymbol{\gamma}^{(j)} \perp \boldsymbol{\gamma}^{(k)}$ $(j \neq k)$ and $\boldsymbol{\gamma}^{(k)\top}\boldsymbol{\Sigma}^*\boldsymbol{\gamma}^{(k)} = 1$, where $\boldsymbol{\Sigma}^*$ is some $p \times p$ covariance representative of the overall study population.

Model (2) involves unknown parameters both in the outcome projection with $\boldsymbol{\Gamma} = [\boldsymbol{\gamma}^{(1)}; \ldots; \boldsymbol{\gamma}^{(d)}] \in \mathbb{R}^{p\times d}$ and the covariates' regression coefficients $\boldsymbol{B} = [\boldsymbol{\beta}^{(1)}; \ldots; \boldsymbol{\beta}^{(d)}]^\top \in \mathbb{R}^{d\times q}$, and joint inference on $\boldsymbol{\Gamma}$ and $\boldsymbol{B}$ is not straightforward under a sequential optimization framework. Thus, in Zhao et al. [2021a,b, 2022], bootstrap-based statistical inference was conducted only on the regression coefficients $\boldsymbol{B}$, and not on the projection dimension reduction coefficients $\boldsymbol{\Gamma}$. The proposed Bayesian estimation approach simultaneously models all the relevant components, and provide a more coherent uncertainty quantification on the parameters $\boldsymbol{\Gamma}$ and $\boldsymbol{B}$, as well as providing the opportunity to account for prior information.

Specifically, extending the formulation (2), we consider a log-variance model of the form:

$$\log \text{var}(\boldsymbol{\Gamma}^\top \boldsymbol{Y}^*_{i,l}) = \text{diag}(\boldsymbol{B}\boldsymbol{x}_i + \boldsymbol{u}_i) \quad (l = 1, \ldots, T_i)(i = 1, \ldots, n), \tag{3}$$

where $\boldsymbol{Y}^*_{i,l} \in \mathbb{R}^p$ is a standardized response signal $\boldsymbol{Y}_{i,l} \in \mathbb{R}^p$ (to be indicated shortly) upon which we apply a dimension reduction projection with $\boldsymbol{\Gamma}$, and subject-specific random effects $\boldsymbol{u}_i \sim N(\boldsymbol{0}, \sigma^2 \boldsymbol{I}_d)$, with some $\sigma^2 > 0$, describe subject-level variation in the variance beyond what is explained by the covariates $\boldsymbol{x}_i$ in the Bayesian paradigm. In Seiler's model (1), the regression component $\boldsymbol{B}\boldsymbol{x}_i\boldsymbol{x}_i^\top\boldsymbol{B}^\top \in \mathbb{R}^{p\times p}$ is of rank-1 (since the vector $\boldsymbol{B}\boldsymbol{x}_i \in \mathbb{R}^p$ is rank-1). On the other hand, model (3) identifies a rank-d (where $d \geq 1$) structure via $\boldsymbol{\Gamma}$ in the outcome space, and thus is potentially more flexible. In particular, by reducing the dimensionality (from p to d) and modeling only the relevant components, the CAP approach avoids the need to work with the full p-by-p covariance matrix, potentially offering computational advantages, and facilitating a more focused analysis. In (3), $\log(\cdot)$ represents the matrix logarithm, and $\text{diag}(\boldsymbol{B}\boldsymbol{x}_i + \boldsymbol{u}_i)$ is the $d \times d$ diagonal matrix with the diagonal elements $\boldsymbol{B}\boldsymbol{x}_i + \boldsymbol{u}_i \in \mathbb{R}^d$.

2 Method

2.1 Covariance model

We consider n subjects, with subject-level covariances between brain activity time series from p ROIs $\{\boldsymbol{\Sigma}_i \in \mathbb{R}^{p\times p}, i = 1, \ldots, n\}$. We consider the associated p-dimensional brain signal vectors $\boldsymbol{Y}_{i,l} \in \mathbb{R}^p$ $(l = 1, \ldots, T_i)$ observed over T_i time points for each subject i $(i = 1, \ldots, n)$, along with subject-level vectors of covariates $\boldsymbol{x}_i \in \mathbb{R}^q$ $(i = 1, \ldots, n)$. As our focus is on the statistical dependency characterized by the covariance between the brain signals (rather than the mean activation), without loss of generality we assume that the observed signal is mean-centered so that $\sum_{l=1}^{T_i} \boldsymbol{Y}_{i,l} = \boldsymbol{0} \in \mathbb{R}^p$ for each subject $(i = 1, \ldots, n)$.

Let us denote the space of $p \times p$ SPD matrices by $\text{Sym}_p^+ = \{\boldsymbol{\Sigma}_i \in \mathbb{R}^{p\times p}\}$. The space Sym_p^+ forms a nonlinear manifold and does not conform to Euclidean geometry; for example, the negative of a SPD matrix and some linear combinations of SPD matrices are not SPD [Schwartzman, 2016], and thus, comparing covariance matrices in the Euclidean vector space is not adequate to capture and preserve the complex structure of the nonlinear manifold. However, Sym_p^+ is a Riemannian manifold under the affine-invariant Riemannian metric [Pennec et al., 2006], whose tangent space (which approximates the local geometry of the manifold at a given point) forms a vector space of symmetric $p \times p$ matrices.

Under the affine-invariant Riemannian metric, we will represent the local differences of covariance matrices $\boldsymbol{\Sigma}_i$ from some fixed reference point $\boldsymbol{\Sigma}^* \in \text{Sym}_p^+$ with vectors in the tangent space (at the identity matrix $\boldsymbol{I}_p$). For a fixed reference point $\boldsymbol{\Sigma}^* \in \text{Sym}_p^+$, the mapping $\phi_{\boldsymbol{\Sigma}^*} : \boldsymbol{\Sigma}_i \to \log(\boldsymbol{\Sigma}^{*-\frac{1}{2}}\boldsymbol{\Sigma}_i\boldsymbol{\Sigma}^{*-\frac{1}{2}})$ [Varoquaux et al., 2010] maps locally the bipoint $\boldsymbol{\Sigma}^*, \boldsymbol{\Sigma}_i \in \text{Sym}_p^+ \times \text{Sym}_p^+$ to an element in the tangent space (at $\boldsymbol{I}_p$), which is no longer linked by the positive definiteness constraint [Pervaiz et al., 2020] and forms a vector space.

A connection that enables a posterior inference in this tangent space is in recognizing that this parametrization $\phi_{\boldsymbol{\Sigma}^*}(\boldsymbol{\Sigma}_i) = \log(\boldsymbol{\Sigma}^{*-\frac{1}{2}}\boldsymbol{\Sigma}_i\boldsymbol{\Sigma}^{*-\frac{1}{2}})$ is equivalent to applying a "whitening" matrix $\boldsymbol{\Sigma}^{*-\frac{1}{2}}$ to the original signal $\boldsymbol{Y}_{i,l} \in \mathbb{R}^p$, i.e.,

$$\boldsymbol{Y}^*_{i,l} := \boldsymbol{\Sigma}^{*-\frac{1}{2}}\boldsymbol{Y}_{i,l},$$

and then working with its log-variance: $\log \text{var}(\boldsymbol{Y}^*_{i,l}) = \log \text{var}(\boldsymbol{\Sigma}^{*-\frac{1}{2}}\boldsymbol{Y}_{i,l}) = \log(\boldsymbol{\Sigma}^{*-\frac{1}{2}}\boldsymbol{\Sigma}_i\boldsymbol{\Sigma}^{*-\frac{1}{2}})(= \phi_{\boldsymbol{\Sigma}^*}(\boldsymbol{\Sigma}_i))$. Thus, we obtain a tangent space parametrization $\phi_{\boldsymbol{\Sigma}^*}(\boldsymbol{\Sigma}_i) = \log \text{var}(\boldsymbol{Y}^*_{i,l})$ of the covariance $\boldsymbol{\Sigma}_i \in \text{Sym}_p^+$ (that can be related with the observable signal $\boldsymbol{Y}^*_{i,l}$ in the tangent space).

In this paper, treating $\{\boldsymbol{\Gamma}^\top\boldsymbol{\Sigma}_i\boldsymbol{\Gamma}\} = \text{Sym}_d^+$ as a Riemannian manifold, we characterize the dimension reduction for $\boldsymbol{\Sigma}_i$ through the bilinear transformation with an unknown orthonormal matrix $\boldsymbol{\Gamma} \in \mathbb{R}^{p\times d}$. In particular, we parametrize the local differences of $\boldsymbol{\Gamma}^\top\boldsymbol{\Sigma}_i\boldsymbol{\Gamma}$ $(= \text{var}(\boldsymbol{\Gamma}^\top\boldsymbol{Y}_{i,l})) \in \text{Sym}_d^+$ from a fixed point $\boldsymbol{\Gamma}^\top\boldsymbol{\Sigma}^*\boldsymbol{\Gamma} \in \text{Sym}_d^+$ by vectors of the tangent space at $\boldsymbol{I}_d$,

$$\phi_{\boldsymbol{\Gamma}^\top\boldsymbol{\Sigma}^*\boldsymbol{\Gamma}} : \boldsymbol{\Gamma}^\top\boldsymbol{\Sigma}_i\boldsymbol{\Gamma} \to \log(\boldsymbol{\Gamma}^\top\boldsymbol{\Sigma}^{*-\frac{1}{2}}\boldsymbol{\Sigma}_i\boldsymbol{\Sigma}^{*-\frac{1}{2}}\boldsymbol{\Gamma}) \quad (= \log \text{var}(\boldsymbol{\Gamma}^\top\boldsymbol{Y}^*_{i,l})) \tag{4}$$

Then, we model the subject-to-subject variability of this tangent space parametrized objects $\phi_{\mathbf{\Gamma}^\top \mathbf{\Sigma}^* \mathbf{\Gamma}}(\mathbf{\Gamma}^\top \mathbf{\Sigma}_i \mathbf{\Gamma}) = \log \text{var}(\mathbf{\Gamma}^\top \boldsymbol{Y}^*_{i,l})$ $(i = 1, \ldots, n)$ in (4) based on $\boldsymbol{x}_i$ $(i = 1, \ldots, n)$ (see model (3)), treating the local difference of $\mathbf{\Gamma}^\top \mathbf{\Sigma}_i \mathbf{\Gamma}$ from $\mathbf{\Gamma}^\top \mathbf{\Sigma}^* \mathbf{\Gamma}$ as a perturbation of $\mathbf{\Gamma}^\top \mathbf{\Sigma}^* \mathbf{\Gamma}$.

Remark 2.1 *Note that we do not use the same definition of the affine-invariant logarithmic mapping as in Pennec et al. [2006], You and Park [2021], since we are interested in mapping to the tangent space at $\boldsymbol{I}_d$, rather than that at $\mathbf{\Gamma}^\top \mathbf{\Sigma}^* \mathbf{\Gamma}$, to extract a statistically independent (diagonal variance) parametrization [Varoquaux et al., 2010] for the model likelihood (see below). Specifically, mapping (4) corresponds to utilizing the whitening transport approach of Ng et al. [2016] which applies log mapping along the identity matrix after removing the effect of a reference covariance.*

To define this tangent space mapping (4), we must find a reference point $\mathbf{\Sigma}^* \in \text{Sym}^+_p$. A sensible point on Sym^+_p is a mean of $\mathbf{\Sigma}_i$ $(i = 1, \ldots, n)$. In this paper, we set $\mathbf{\Sigma}^* = \frac{1}{n} \sum_{i=1}^n \frac{1}{T_i} \sum_{l=1}^{T_i} \boldsymbol{Y}_{i,l} \boldsymbol{Y}_{i,l}^\top$, i.e., the sample marginal covariance matrix computed across the subjects $i = 1, \ldots, n$.

To conduct statistical inference on the dimension reducing orthonormal matrix $\mathbf{\Gamma}$ and the parameter $\boldsymbol{B}$ in model (3), we shall use the following d-dimensional Gaussian likelihood model:

$$\mathbf{\Gamma}^\top \boldsymbol{Y}^*_{i,l} \sim \mathcal{N}_d(\mathbf{0}, \mathbf{\Lambda}_i) \qquad \text{with variance } \mathbf{\Lambda}_i = \begin{bmatrix} \exp(\boldsymbol{x}_i^\top \boldsymbol{\beta}^{(1)} + u_i^{(1)}) & 0 & 0 \\ 0 & \exp(\boldsymbol{x}_i^\top \boldsymbol{\beta}^{(2)} + u_i^{(2)}) & 0 \\ 0 & 0 & \exp(\boldsymbol{x}_i^\top \boldsymbol{\beta}^{(d)} + u_i^{(d)}) \end{bmatrix}, \tag{5}$$

that is, $\log \mathbf{\Lambda}_i = \text{diag}(\boldsymbol{B}\boldsymbol{x}_i + \boldsymbol{u}_i) \in \mathbb{R}^{d \times d}$ (a log-linear model for variance), where $\boldsymbol{B} = [\boldsymbol{\beta}^{(1)}; \ldots; \boldsymbol{\beta}^{(d)}]^\top \in \mathbb{R}^{d \times q}$ is the regression coefficient matrix associated with covariates $\boldsymbol{x}_i \in \mathbb{R}^q$, and $\boldsymbol{u}_i = [u_i^{(1)}, \ldots, u_i^{(d)}]^\top \in \mathbb{R}^d$ is the subject-level noise vector with $u_i^{(k)} \sim N(0, \sigma^2)$. The prior distribution on $\mathbf{\Gamma}$ is a matrix angular central Gaussian (MACG) [Chikuse, 1990, Jupp and Mardia, 1999] with some hyperparameter $\mathbf{\Psi} \in \text{Sym}^+_p$ (see Section 2.2 below).

Remark 2.2 *The variance model (5) should be distinguished from the principal component (PC) regression that relates $\boldsymbol{x}_i$ with the PCs $\mathbf{\Gamma}^\top \boldsymbol{Y}^*_{i,l} \in \mathbb{R}^d$, as our study interest is the association between the covariate $\boldsymbol{x}_i$ and the variance of the PCs, that is, var$(\mathbf{\Gamma}^\top \boldsymbol{Y}^*_{i,l}) \in Sym^+_d$, rather than that between $\boldsymbol{x}_i$ and the PCs $\mathbf{\Gamma}^\top \boldsymbol{Y}^*_{i,l} \in \mathbb{R}^d$ themselves.*

Remark 2.3 *In conducting the posterior inference (described in Section 2.2), the assumption that we make is that the set of orthogonal directions $\mathbf{\Gamma}$ for $\boldsymbol{Y}^*_{i,l} \in \mathbb{R}^p$ is sufficient for characterizing the association between var$(\boldsymbol{Y}^*_{i,l})$ and the covariate $\boldsymbol{x}_i$.*

Upon back-transforming the tangent space parametrization (4) into the original space Sym^+_d by applying the affine-invariant *exponential* map to $\phi_{\mathbf{\Gamma}^\top \mathbf{\Sigma}^* \mathbf{\Gamma}}(\mathbf{\Gamma}^\top \mathbf{\Sigma}_i \mathbf{\Gamma}) = \log \text{var}(\mathbf{\Gamma}^\top \boldsymbol{Y}^*_{i,l})$, we have, under model (5), the variance model

$$\mathbf{\Gamma}^\top \mathbf{\Sigma}_i \mathbf{\Gamma} = \mathbf{\Gamma}^\top \mathbf{\Sigma}^{*\frac{1}{2}} \exp(\text{diag}(\boldsymbol{B}\boldsymbol{x}_i + \boldsymbol{u}_i)) \mathbf{\Sigma}^{*\frac{1}{2}} \mathbf{\Gamma}, \tag{6}$$

where $\mathbf{\Sigma}^*$ is the fixed reference point employed in the tangent space parametrization. In model (6), the population-level covariance $\mathbf{\Gamma}^\top \mathbf{\Sigma}^* \mathbf{\Gamma} \in \mathbb{R}^{d \times d}$ in which the data-driven orthogonal $\mathbf{\Gamma}$ characterizes the principal modes of the variability within $\mathbf{\Sigma}_i$ associated with covariates $\boldsymbol{x}_i$, is scaled by the subject-level variance $\exp(\text{diag}(\boldsymbol{B}\boldsymbol{x}_i + \boldsymbol{u}_i)) \in \mathbb{R}^{d \times d}$. By making posterior inference on the parameters of the model (5), we can make inference on the parameters in (6).

2.2 Posterior inference

Upon diagonalization via the dimension reduction matrix $\mathbf{\Gamma}$, the model (5) associated with the variance $\mathbf{\Lambda}_i$ is a log-linear model, $\log \mathbf{\Lambda}_i = \text{diag}(\boldsymbol{B}\boldsymbol{x}_i + \boldsymbol{u}_i)$ $(i = 1, \ldots, n)$, modeled based on the covariates $\boldsymbol{x}_i$. Let us use $\boldsymbol{Y}^*$ to represent the collection $\{\boldsymbol{Y}^*_{i,l} \ (= \mathbf{\Sigma}^{*-\frac{1}{2}} \boldsymbol{Y}_{i,l}) \in \mathbb{R}^p, i = 1, \ldots, n_i, l = 1, \ldots, n_i\}$ and $\mathbf{\Lambda}$ to represent the collection $\{\mathbf{\Lambda}_i \in \mathbb{R}^{d \times d}, i = 1, \ldots, n\}$. Then, the posterior distribution of the model parameters, $(\mathbf{\Gamma}, \mathbf{\Lambda}, \boldsymbol{B}, \sigma^2)$, can be expressed in terms the product of the likelihood and the prior,

$$p(\mathbf{\Gamma}, \mathbf{\Lambda}, \boldsymbol{B}, \sigma^2 | \boldsymbol{Y}^*) \quad \propto \quad p(\boldsymbol{Y}^* | \mathbf{\Gamma}, \mathbf{\Lambda}, \boldsymbol{B}, \sigma^2) p(\mathbf{\Gamma}, \mathbf{\Lambda}, \boldsymbol{B}, \sigma^2), \tag{7}$$

where the model likelihood $p(\boldsymbol{Y}^* | \mathbf{\Gamma}, \mathbf{\Lambda}, \boldsymbol{B}, \sigma^2)$ is specified based on the Gaussian model (5),

$$\begin{aligned} p(\boldsymbol{Y}^* | \mathbf{\Gamma}, \mathbf{\Lambda}, \boldsymbol{B}, \sigma^2) = p(\boldsymbol{Y}^* | \mathbf{\Gamma}, \mathbf{\Lambda}) \ &\propto \ \prod_{i=1}^n \prod_{l=1}^{T_i} p(\mathbf{\Gamma}^\top \boldsymbol{Y}^*_{i,l} | \mathbf{\Gamma}, \mathbf{\Lambda}_i) \\ &\propto \ \prod_{i=1}^n \prod_{l=1}^{T_i} \exp\left\{ -\frac{1}{2} \log |\mathbf{\Lambda}_i| - \frac{1}{2} \text{tr}(\mathbf{\Lambda}_i^{-1} \mathbf{\Gamma}^\top \boldsymbol{Y}^*_{i,l} \boldsymbol{Y}^{*\top}_{i,l} \mathbf{\Gamma}) \right\}, \end{aligned}$$

and the prior $p(\boldsymbol{\Gamma}, \boldsymbol{\Lambda}, \boldsymbol{B}, \sigma^2)$ is specified as

$$\begin{aligned} p(\boldsymbol{\Gamma}, \boldsymbol{\Lambda}, \boldsymbol{B}, \sigma^2) &= p(\boldsymbol{\Gamma}, \boldsymbol{B}, \sigma^2) p(\boldsymbol{\Lambda} | \boldsymbol{\Gamma}, \boldsymbol{B}, \sigma^2) \\ &\propto\ p(\boldsymbol{\Gamma}) p(\boldsymbol{B}) p(\sigma^2) \exp\left\{ -\frac{1}{2\sigma^2} \sum_{i=1}^{n} (\boldsymbol{\lambda}_i - \boldsymbol{B}\boldsymbol{x}_i)^\top (\boldsymbol{\lambda}_i - \boldsymbol{B}\boldsymbol{x}_i) - \frac{n}{2} \log \sigma^2 \right\}, \end{aligned} \tag{8}$$

where $\boldsymbol{\lambda}_i \in \mathbb{R}^d$ is the vector of the diagonal elements of $\log \boldsymbol{\Lambda}_i \in \mathbb{R}^{d \times d}$, and independent priors $p(\boldsymbol{\Gamma}, \boldsymbol{B}, \sigma^2) = p(\boldsymbol{\Gamma}) p(\boldsymbol{B}) p(\sigma^2)$ are used for the parameters $\boldsymbol{\Gamma}$, $\boldsymbol{B}$ and σ^2. We use a mean-zero (weakly informative) matrix Gaussian prior on $\boldsymbol{B} \in \mathbb{R}^{d \times q}$ (with element-wise standard deviation 2.5) and a (weakly informative) mean-one exponential prior on $\sigma^2 > 0$. The prior on $\boldsymbol{\Gamma}$ is MACG$(\boldsymbol{\Gamma} | \boldsymbol{\Psi})$ with a hyperparameter $\boldsymbol{\Psi} \in \text{Sym}_p^+$, whose density is

$$p(\boldsymbol{\Gamma} | \boldsymbol{\Psi}) = |\boldsymbol{\Psi}|^{-d/2} |\boldsymbol{\Gamma}^\top \boldsymbol{\Psi}^{-1} \boldsymbol{\Gamma}|^{-p/2} \tag{9}$$

where $\boldsymbol{\Gamma}$ is in the space of $p \times d$ orthonormal matrices. Note that an orthonormal random matrix $\boldsymbol{\Gamma} \in \mathbb{R}^{p \times d}$ is said to be distributed as MACG$(\boldsymbol{\Gamma} | \boldsymbol{\Psi})$ (9), if $\boldsymbol{\Gamma}$ is equal in distribution ($\stackrel{d}{=}$) to the orthonormal matrix $\boldsymbol{\Gamma}_U := \boldsymbol{U}(\boldsymbol{U}^\top \boldsymbol{U})^{-1/2} \in \mathbb{R}^{p \times d}$, where

$$\boldsymbol{U} \sim \mathcal{N}_{p \times d}(\boldsymbol{0}_{p \times d}, \boldsymbol{\Psi}, \boldsymbol{I}), \tag{10}$$

(i.e., $\boldsymbol{U}$ is a matrix Gaussian with row covariance $\boldsymbol{\Psi} \in \mathbb{R}^{p \times p}$ and identity column covariance $\boldsymbol{I} \in \mathbb{R}^{d \times d}$). Accordingly, the orthonormal matrix $\boldsymbol{\Gamma} (\stackrel{d}{=} \boldsymbol{\Gamma}_U := \boldsymbol{U}(\boldsymbol{U}^\top \boldsymbol{U})^{-1/2})$ represents the "orientation" of $\boldsymbol{U} \in \mathbb{R}^{p \times d}$. We can incorporate prior structure such as spatial correlation among the p regions through the row covariance $\boldsymbol{\Psi}$.

2.2.1 Posterior computation via polar expansion

A MCMC sampling for $\boldsymbol{\Gamma}$ from the posterior (7) is challenging due to the restriction that $\boldsymbol{\Gamma}$ is in a Stiefel manifold. To get around with this constraint, we will use polar expansion to transform the orthonormal $\boldsymbol{\Gamma}$ to an unconstrained object $(\boldsymbol{U})$. Generally, "parameter expansion" of a statistical model refers to methods which expand the parameter space by introducing redundant working parameters for computational purposes [Jauch et al., 2021]. By polar decomposition [Higham, 1986], any arbitrary (random) matrix $\boldsymbol{U} \in \mathbb{R}^{p \times d}$ can be decomposed into two components

$$\boldsymbol{U} = \boldsymbol{\Gamma}_U \boldsymbol{S}_U \tag{11}$$

(almost surely), where the first component $\boldsymbol{\Gamma}_U := \boldsymbol{U}(\boldsymbol{U}^\top \boldsymbol{U})^{-1/2} \in \mathbb{R}^{p \times d}$ is an orthonormal (i.e., a rotation) matrix, and the second component $\boldsymbol{S}_U := (\boldsymbol{U}^\top \boldsymbol{U})^{1/2} \in \mathbb{R}^{d \times d}$ is a symmetric nonnegative (i.e., a stretch tensor) matrix.

With a matrix Gaussian prior on $\boldsymbol{U}$, we have a MACG prior such that $\boldsymbol{\Gamma} \stackrel{d}{=} \boldsymbol{\Gamma}_U$. Accordingly, we can write the posterior by $p(\boldsymbol{\Gamma}, \boldsymbol{\Lambda}, \boldsymbol{B}, \sigma^2 | \boldsymbol{Y}^*) = p(\boldsymbol{\Gamma}_U, \boldsymbol{\Lambda}, \boldsymbol{B}, \sigma^2 | \boldsymbol{Y}^*)$. Then, via polar expansion (11), we can work with the expanded posterior

$$p(\boldsymbol{\Gamma}_U, \boldsymbol{\Lambda}, \boldsymbol{B}, \sigma^2 | \boldsymbol{Y}^*) \quad \rightarrow \quad p(\boldsymbol{U}, \boldsymbol{\Lambda}, \boldsymbol{B}, \sigma^2 | \boldsymbol{Y}^*)$$

where we "parameter expand" from an orthonormal $\boldsymbol{\Gamma}_U$ to an unconstrained $\boldsymbol{U}$, in which

$$\begin{aligned} p(\boldsymbol{U}, \boldsymbol{\Lambda}, \boldsymbol{B}, \sigma^2 | \boldsymbol{Y}^*) &\propto p(\boldsymbol{Y}^* | \boldsymbol{U}, \boldsymbol{\Lambda}) p(\boldsymbol{U}, \boldsymbol{\Lambda}, \boldsymbol{B}, \sigma^2) = p(\boldsymbol{Y}^* | \boldsymbol{\Gamma}_U, \boldsymbol{\Lambda}) p(\boldsymbol{U}, \boldsymbol{\Lambda}, \boldsymbol{B}, \sigma^2) \\ &\propto \prod_{i=1}^{n} \prod_{l=1}^{T_i} \exp\left\{ -\frac{1}{2} \log |\boldsymbol{\Lambda}_i| - \frac{1}{2} \text{tr}(\boldsymbol{\Lambda}_i^{-1} \boldsymbol{\Gamma}_U^\top \boldsymbol{Y}_{i,l}^* \boldsymbol{Y}_{i,l}^{*\top} \boldsymbol{\Gamma}_U) \right\} p(\boldsymbol{U}) p(\boldsymbol{B}) p(\sigma^2) p(\boldsymbol{\Lambda} | \boldsymbol{U}, \boldsymbol{B}, \sigma^2). \end{aligned} \tag{12}$$

We first approximate samples from the posterior distribution $p(\boldsymbol{U}, \boldsymbol{\Lambda}, \boldsymbol{B}, \sigma^2 | \boldsymbol{Y}^*)$ using MCMC and then conduct the polar decomposition (11) to approximate samples from the posterior distribution associated with $\boldsymbol{\Gamma}_U \stackrel{d}{=} \boldsymbol{\Gamma}$. Specifically, given a Markov chain $\{\boldsymbol{U}_t, \boldsymbol{\Lambda}_t, \boldsymbol{B}_t, \sigma_t\}$ whose stationary distribution is proportional to (12), we approximate the marginal posterior distribution of $\boldsymbol{\Gamma}$ by $\{\boldsymbol{\Gamma}_t\}$ where $\boldsymbol{\Gamma}_t = \boldsymbol{U}_t(\boldsymbol{U}_t^\top \boldsymbol{U}_t)^{-1/2}$ for each t, that yields approximate samples from the posterior distribution of $(\boldsymbol{\Gamma}, \boldsymbol{\Lambda}, \boldsymbol{B}, \sigma^2)$. As in any PCA-type analysis, there is a sign non-identifiability of $\boldsymbol{\Gamma}$; the non-identifiability of matrix $\boldsymbol{\Gamma}$ up to random sign changes for each component. That is, the component vector $\boldsymbol{\gamma}^{(k)}$ and $-\boldsymbol{\gamma}^{(k)}$ correspond to the same direction. We need to align the posterior samples coming from multiples chains based on Procrustes alignment. In this paper, we obtain an MCMC approximation to the posterior distribution of the parameters $(\boldsymbol{U}, \boldsymbol{\Lambda}, \boldsymbol{B}, \sigma)$ using an adaptive Hamiltonian Monte Carlo (HMC) sampler [Neal, 2011] with automatic differentiation and adaptive tuning functionality, as implemented in Stan [Stan Development Team, 2023].

Unlike ICA, where the order of the extracted components is relatively arbitrary, the components specified by the orthonormal matrix $\boldsymbol{\Gamma}$ can be rank-ordered according to the proportion of variance of the expected log-variance $E[\log \Lambda_i^{(k)} | \boldsymbol{Y}^*]$

$(k = 1, \ldots, d)$ they explain across the samples $i = 1, \ldots, n$. Here, $\log \Lambda_i^{(k)} = \boldsymbol{x}_i^\top \boldsymbol{\beta}^{(k)} + u_i^{(k)}$ $(k = 1, \ldots, d)$ is the $(k$th) diagonal element of the log-variance $\log \boldsymbol{\Lambda}_i$. Thus, we sort the estimated d components on a decreasing order, with respect to the magnitude of the sample variance $V^{(k)} = \sum_{i=1}^n \left\{ E[\log \Lambda_i^{(k)} | \boldsymbol{Y}^*] - \frac{1}{n} \sum_{i=1}^n E[\log \Lambda_i^{(k)} | \boldsymbol{Y}^*] \right\}^2$ of the expected log-variance $E[\log \Lambda_i^{(k)} | \boldsymbol{Y}^*]$ $(k = 1, \ldots, d)$. This sample variance $V^{(k)}$ quantifies the between-subject variability in the log-variance of the multivariate signal captured by the kth component.

2.3 Determination of the number d of the components

The number of components d is determined based on a metric that measures the level of "deviation from diagonality" (DfD) of the sample version of $\boldsymbol{\Lambda}_i$ in (5), as in Zhao et al. [2021a]. If the estimated variance $\widehat{\text{var}}(\boldsymbol{\Gamma}^\top \boldsymbol{Y}_{i,l}^*) = \boldsymbol{\Gamma}^\top \boldsymbol{\Sigma}^{*-\frac{1}{2}} \widehat{\boldsymbol{\Sigma}}_i \boldsymbol{\Sigma}^{*-\frac{1}{2}} \boldsymbol{\Gamma} = \widehat{\boldsymbol{\Lambda}}_i$ of the rotated matrix $\boldsymbol{\Gamma}^\top \boldsymbol{Y}_{i,l}^*$ deviates from the diagonality assumed in model (5), then the following quantity

$$\log \text{DfD}(\{\widehat{\boldsymbol{\Lambda}}_i\}) := \frac{1}{n} \sum_{i=1}^n T_i \left(\log|\text{Diag}(\widehat{\boldsymbol{\Lambda}}_i)| - \log|\widehat{\boldsymbol{\Lambda}}_i| \right), \tag{13}$$

where $\text{Diag}(\widehat{\boldsymbol{\Lambda}}_i)$ is a $d \times d$ diagonal matrix with its diagonal elements given by the diagonal elements of $\widehat{\boldsymbol{\Lambda}}_i$, and the determinants $|\text{Diag}(\widehat{\boldsymbol{\Lambda}}_i)|$ and $|\widehat{\boldsymbol{\Lambda}}_i|$ correspond to the determinants of the $d \times d$ matrices $\text{diag}(\widehat{\boldsymbol{\Lambda}}_i)$ and $\widehat{\boldsymbol{\Lambda}}_i$, respectively, tends to deviate from 0. From Hadamard's inequality, we have $\log \text{DfD}(\{\widehat{\boldsymbol{\Lambda}}_i\}) \geq 0$ [Zhao et al., 2021a, Flury and Gautschi, 1986], and the equality occurs if the matrix $\widehat{\boldsymbol{\Lambda}}_i$ is perfectly diagonal. The requirement for $\widehat{\text{var}}(\boldsymbol{\Gamma}^\top \boldsymbol{Y}_{i,l}^*) = \widehat{\boldsymbol{\Lambda}}_i$ to be diagonal by model (5) may become more stringent as the dimensionality d increases [Zhao et al., 2021a], and thus, with a too large number of components d, the quantity $\log \text{DfD}(\{\widehat{\boldsymbol{\Lambda}}_i\})$ tends to deviate from 0.

We will utilize posterior samples from MCMC to compute the posterior mean of (13), $E[\log \text{DfD}(\{\widehat{\boldsymbol{\Lambda}}_i\}) | \boldsymbol{Y}^*]$, by using the HMC sampler outputs on $\widehat{\boldsymbol{\Lambda}}_i^{(t)} = \boldsymbol{\Gamma}^{(t)\top} \boldsymbol{\Sigma}^{*-\frac{1}{2}} \widehat{\boldsymbol{\Sigma}}_i \boldsymbol{\Sigma}^{*-\frac{1}{2}} \boldsymbol{\Gamma}^{(t)}$ for each subject i $(i = 1, \ldots, n)$, where $\boldsymbol{\Gamma}^{(t)}$ is the tth posterior sampler output for $\boldsymbol{\Gamma}$ from the Markov chain, and $\widehat{\boldsymbol{\Sigma}}_i (= \frac{1}{T_i} \sum_{l=1}^{T_i} \boldsymbol{Y}_{i,l}^* \boldsymbol{Y}_{i,l}^{*\top})$ is the sample covariance matrix for subject i. Heuristically, we can increase the projection dimension from 1 to some reasonable number, $\check{d} (\leq p)$, and choose a suitable number right before a large jump in the metric, or identify an appropriate number by finding the largest d such that the metric $E[\log \text{DfD}(\{\widehat{\boldsymbol{\Lambda}}_i\}) | \boldsymbol{Y}^*]$ is less than some threshold, i.e., choose the largest d such that $E[\log \text{DfD}(\{\widehat{\boldsymbol{\Lambda}}_i\}) | \boldsymbol{Y}^*] \leq c$ for some cutoff value c. In Supplementary Materials, we report the proportion of the correctly identified number of the components from simulation experiments with $c = 1.5$, demonstrating the performance of this approach to determine the number of components in the model.

3 Simulation illustration

3.1 Simulation setup

For each unit (subject) i $(i = 1, \ldots, n)$, we simulate a set of outcome signals $\boldsymbol{Y}_{i,l} \in \mathbb{R}^p$ $(l = 1, \ldots, T_i)$ from a Gaussian distribution with mean zero and $p \times p$ unit-specific covariance $\boldsymbol{\Sigma}_i$. In our simulation illustration, we vary $n \in \{50, 100, 200, 400\}$, $T_i \in \{10, 20, 40\}$, and $p \in \{5, 20\}$.

We first consider the case with $p = 5$. We specify the unit-specific covariance $\boldsymbol{\Sigma}_i$ based on the spectral decomposition

$$\boldsymbol{\Sigma}_i = \widetilde{\boldsymbol{\Gamma}}_i \widetilde{\boldsymbol{\Lambda}}_i \widetilde{\boldsymbol{\Gamma}}_i^\top \quad (i = 1, \ldots, n), \tag{14}$$

where the $p \times p$ diagonal matrix $\widetilde{\boldsymbol{\Lambda}}_i = \exp(\text{diag}(\tilde{\boldsymbol{B}} \boldsymbol{x}_i + \tilde{\boldsymbol{u}}_i))$ is based on the model

$$\tilde{\boldsymbol{B}} \boldsymbol{x}_i + \tilde{\boldsymbol{u}}_i = \underset{p \times 3}{\begin{pmatrix} 1 & 0 & 0 \\ 1 & 0.5 & -0.5 \\ 1 & -0.3 & 0.3 \\ 1 & 0 & 0 \\ 1 & 0 & 0 \end{pmatrix}} \underset{3 \times 1}{\begin{pmatrix} 1 \\ x_{i1} \\ x_{i2} \end{pmatrix}} + \underset{p \times 1}{\begin{pmatrix} \tilde{u}_{i1} \\ \tilde{u}_{i2} \\ \tilde{u}_{i3} \\ \tilde{u}_{i4} \\ \tilde{u}_{i5} \end{pmatrix}} \in \mathbb{R}^p, \tag{15}$$

with $x_{i1} \sim \text{Bernulli}(0.5)$, $x_{i2} \sim N(0, 1^2)$, and $\tilde{u}_{ik} \sim N(0, 0.5^2)$ $(k = 1, \ldots, p)$ generated independently with each other, and the $p \times p$ orthonormal matrix $\widetilde{\boldsymbol{\Gamma}}_i$ is based on the population level orthonormal matrix

$\widetilde{\mathbf{\Gamma}} = (\boldsymbol{\gamma}_1, \boldsymbol{\gamma}^{(1)}, \boldsymbol{\gamma}^{(2)}, \boldsymbol{\gamma}_4, \boldsymbol{\gamma}_5)$:

$$\widetilde{\mathbf{\Gamma}} = \begin{array}{c} \begin{matrix} \boldsymbol{\gamma}_1 & \boldsymbol{\gamma}^{(1)} & \boldsymbol{\gamma}^{(2)} & \boldsymbol{\gamma}_4 & \boldsymbol{\gamma}_5 \end{matrix} \\ \begin{pmatrix} 0.447 & 0.447 & 0.447 & 0.447 & 0.447 \\ 0.447 & -0.862 & 0.138 & 0.138 & 0.138 \\ 0.447 & 0.138 & -0.862 & 0.138 & 0.138 \\ 0.447 & 0.138 & 0.138 & -0.862 & 0.138 \\ 0.447 & 0.138 & 0.138 & 0.138 & -0.862 \end{pmatrix}_{p \times p} \end{array}, \tag{16}$$

which is then transformed into the subject i-specific eigenmatrix $\widetilde{\mathbf{\Gamma}}_i$,

$$\widetilde{\mathbf{\Gamma}}_i = (\mathbf{\Omega}\boldsymbol{a}_{i1} \quad \boldsymbol{\gamma}^{(1)} \quad \boldsymbol{\gamma}^{(2)} \quad \mathbf{\Omega}\boldsymbol{a}_{i2} \quad \mathbf{\Omega}\boldsymbol{a}_{i3}) \quad (i = 1, \ldots, n), \tag{17}$$

where the subject-specific eigenvectors $(\mathbf{\Omega}\boldsymbol{a}_{i1} \quad \mathbf{\Omega}\boldsymbol{a}_{i2} \quad \mathbf{\Omega}\boldsymbol{a}_{i3})$ are obtained based on a randomly generated 3×3 orthonormal matrix $\boldsymbol{A}_i = (\boldsymbol{a}_{i1} \quad \boldsymbol{a}_{i2} \quad \boldsymbol{a}_{i3})$ (from the von Mises-Fisher distribution to $\mathbf{\Omega} := (\boldsymbol{\gamma}_1 \quad \boldsymbol{\gamma}_4 \quad \boldsymbol{\gamma}_5)$. Since only the 2nd and 3rd rows of the matrix $\tilde{\boldsymbol{B}}$ in (15) are associated with the covariates $\{x_{i1}, x_{i2}\}$, only the 2nd and 3rd columns of the eigenvector matrix in (17) (i.e., the eigenvectors $\boldsymbol{\gamma}^{(1)}$ and $\boldsymbol{\gamma}^{(2)}$) capture the information related to the covariates $\{x_{i1}, x_{i2}\}$, whereas the other eigenvectors $(\mathbf{\Omega}\boldsymbol{a}_{i1} \quad \mathbf{\Omega}\boldsymbol{a}_{i2} \quad \mathbf{\Omega}\boldsymbol{a}_{i3})$ do not capture the information related to the covariates.

The model indicates that, upon applying the dimension reduction matrix $\mathbf{\Gamma} = (\boldsymbol{\gamma}^{(1)}, \boldsymbol{\gamma}^{(2)}) \in \mathbb{R}^{p \times 2}$ to the vector $\boldsymbol{Y}_{i,l} \in \mathbb{R}^p$, we have the reduced form $\mathbf{\Gamma}^\top \boldsymbol{Y}_{i,l} \sim N_2(\boldsymbol{0}, \mathbf{\Gamma}^\top \mathbf{\Sigma}_i \mathbf{\Gamma})$, where $\mathbf{\Gamma}^\top \mathbf{\Sigma}_i \mathbf{\Gamma} = \exp(\mathrm{diag}(\boldsymbol{B}\boldsymbol{x}_i + \boldsymbol{u}_i))$, in which $\boldsymbol{B}\boldsymbol{x}_i = \begin{pmatrix} 1 & 0.5 & -0.5 \\ 1 & -0.3 & 0.3 \end{pmatrix} \boldsymbol{x}_i = \begin{pmatrix} \beta_0^{(1)} + (x_{i1}\ x_{i2})\boldsymbol{\beta}^{(1)} \\ \beta_0^{(2)} + (x_{i1}\ x_{i2})\boldsymbol{\beta}^{(2)} \end{pmatrix} \in \mathbb{R}^2$ and $\boldsymbol{u}_i = (u_i^{(1)}, u_i^{(2)}) \in \mathbb{R}^2$ with $u_i^{(k)} \sim N(0, 0.5^2)$, the same form assumed in the proposed dimension reduction model (6) for $\mathbf{\Sigma}_i$ with $d = 2$, up to a multiplicative factor of $\mathbf{\Gamma}^\top \mathbf{\Sigma}^* \mathbf{\Gamma} \in \mathrm{Sym}_d^+$. Here, this multiplicative factor (stretch tensor) $\mathbf{\Gamma}^\top \mathbf{\Sigma}^* \mathbf{\Gamma}$, which was introduced in our estimation model due to the tangent space parametrization at $\mathbf{\Gamma}^\top \mathbf{\Sigma}^* \mathbf{\Gamma}$ (where $\mathbf{\Sigma}^*$ corresponds to the sample marginal covariance computed on the training sample for each simulation run), only shifts the intercepts $\beta_0^{(1)}$ and $\beta_0^{(2)}$ of the data generation model. Specifically, the model in the tangent space given a reference point $\mathbf{\Sigma}^* \in \mathrm{Sym}_p^+$ parametrizes the intercepts as $\beta_0^{(1)*} := \beta_0^{(1)} + \log(\boldsymbol{\gamma}^{(1)\top} \mathbf{\Sigma}^{*-1} \boldsymbol{\gamma}^{(1)})$ and $\beta_0^{(2)*} := \beta_0^{(2)} + \log(\boldsymbol{\gamma}^{(2)\top} \mathbf{\Sigma}^{*-1} \boldsymbol{\gamma}^{(2)})$.

For the case with $p = 20$, for each simulation run, we randomly generate a 20×20 orthonormal matrix $\widetilde{\mathbf{\Gamma}}$ for (16) and subject-specific 20×18 orthonormal matrices $\boldsymbol{A}_i$ from the von Mises-Fisher distribution, to define the subject-specific eigenvectors $\widetilde{\mathbf{\Gamma}}_i$ in (17) but with $p = 20$, in which the vectors $(\boldsymbol{\gamma}^{(1)}, \boldsymbol{\gamma}^{(2)})$ are common eigenvectors whose eigenvalues vary with the covariates $\{x_{i1}, x_{i2}\}$. To specify the matrix $\widetilde{\boldsymbol{B}}$ in (15) for $p = 20$, we augment the matrix with 15 more rows where each row is $(1, 0, 0)$, and we set $\tilde{\boldsymbol{u}}_i \in \mathbb{R}^{20}$ where $\tilde{u}_{ik} \sim N(0, 0.5^2)$.

3.2 Evaluation metric

We run the simulation 100 times. For each simulation run, we compute, as evaluation metrics, $|\langle \widehat{\boldsymbol{\gamma}}^{(k)}, \boldsymbol{\gamma}^{(k)} \rangle|$ and the mean squared error (MSE) $\|\widehat{\boldsymbol{\beta}}^{(k)} - \boldsymbol{\beta}^{(k)}\|^2/2$ associated with each component, and $|\widehat{\sigma} - \sigma|$ (where $\sigma = 0.5$) for the random effect standard deviation, where $\widehat{\cdot}$ represents the posterior mean of $\cdot$. We also report the estimation performance for the intercepts $\beta_0^{(1)*}$ and $\beta_0^{(2)*}$ in terms of MSE. Note that, in the estimation, the intercept term $\boldsymbol{\beta}_0^* = (\beta_0^{(1)*}, \beta_0^{(2)*})^\top$ was reparametrized due to the tangent space parametrization given a fixed point $\mathbf{\Sigma}^*$, where $\mathbf{\Sigma}^*$ was computed based on the sample. Additionally, to assess whether the credible intervals provide reasonably correct coverage for the true values of the parameters, we evaluate the posterior credible intervals of the model parameters ($\boldsymbol{\gamma}^{(k)}$, $\boldsymbol{\beta}^{(k)}$ and σ) with respect to the frequentist's coverage proportion. For each simulation run, we estimate the posterior distribution of the parameters based on the simulated data and calculate the 95% posterior credible intervals for the parameters, and then evaluate how often the credible intervals contain the true parameter values.

3.3 Simulation results

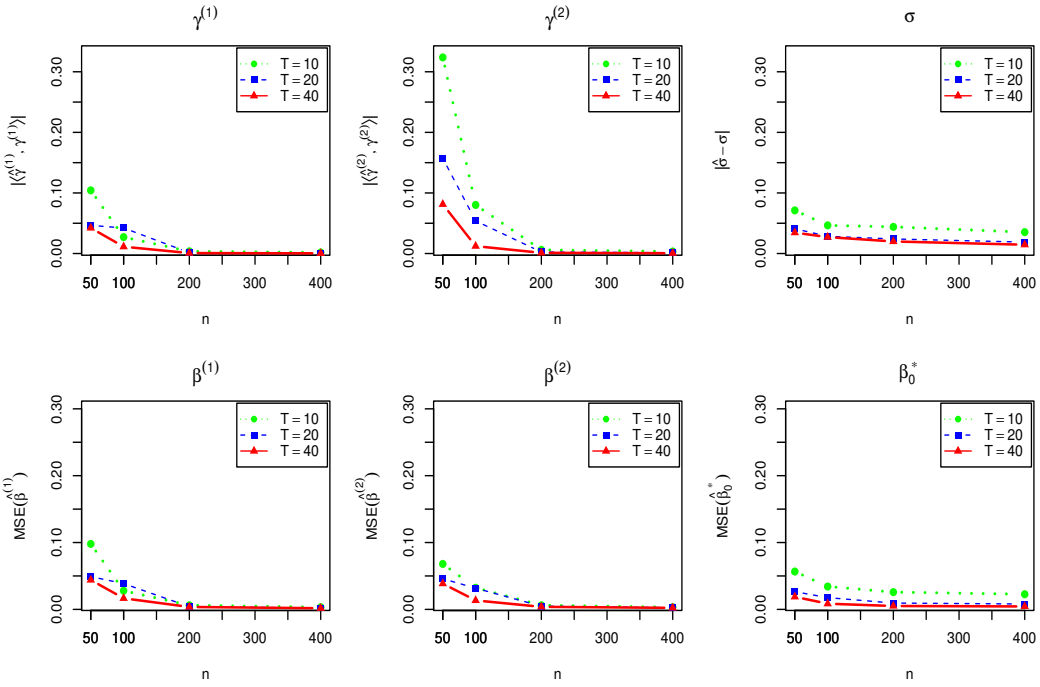

Figure 1: The model parameter estimation performance for $p = 5$ case, for the loading coefficient vectors $\boldsymbol{\gamma}^{(k)}$ $(k = 1, 2)$, the standard deviation of the subject-level parameters σ, and the regression coefficients $\boldsymbol{\beta}^{(k)}$ $(k = 1, 2)$ and the intercept $\boldsymbol{\beta}_0^*$, averaged across 100 simulation replications, with varying $n \in \{50, 100, 200, 400\}$ and $T \in \{10, 20, 40\}$.

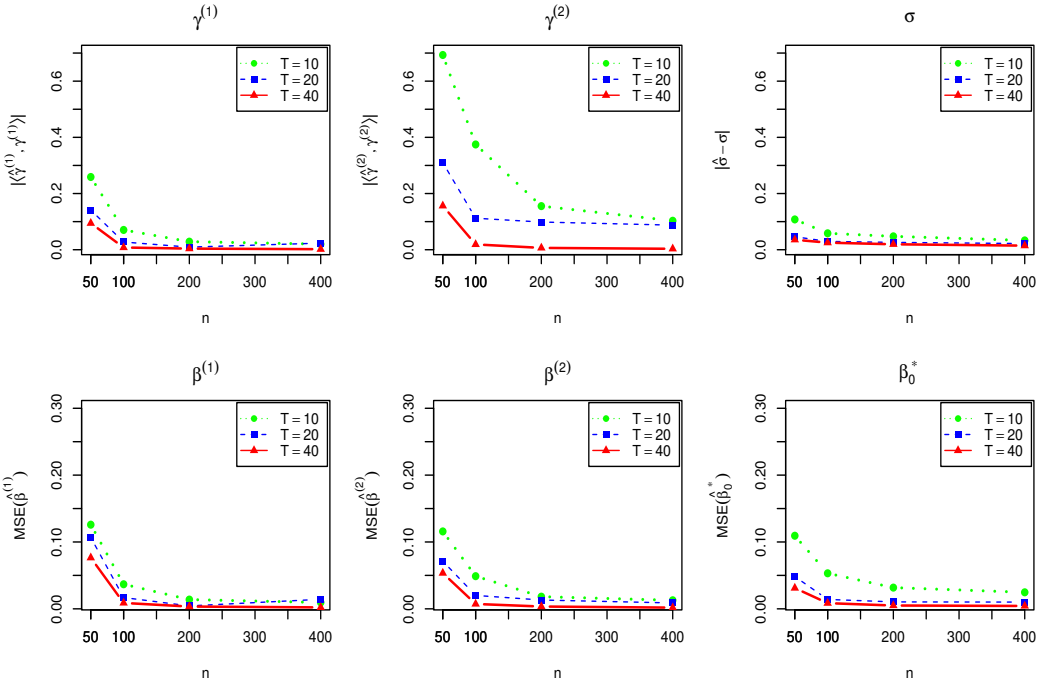

Figure 2: The model parameter estimation performance for $p = 20$ case, for the loading coefficient vectors $\boldsymbol{\gamma}^{(k)}$ $(k = 1, 2)$, the standard deviation of the subject-level parameters σ, and the regression coefficients $\boldsymbol{\beta}^{(k)}$ $(k = 1, 2)$ and the intercept $\boldsymbol{\beta}_0^*$, averaged across 100 simulation replications, with varying $n \in \{50, 100, 200, 400\}$ and $T \in \{10, 20, 40\}$.

The results in Figures 1 and 2 indicate that generally, as the sample sizes n (i.e., the number of subjects) and T (i.e., the number of time points) increase, the estimation performance improves. Although a larger sample size provides more information and leads to more precise estimates, the general improvement depends on each component's effect size magnitude and the dimensionality p. In Figures 1 and 2, the parameter estimation associated with the first component (i.e., $\boldsymbol{\gamma}^{(1)}$ and $\boldsymbol{\beta}^{(1)}$) tends to have a better performance compared to that associated with the second component (i.e., $\boldsymbol{\gamma}^{(2)}$ and $\boldsymbol{\beta}^{(2)}$), as the first component's underlying covariates' effect magnitude in explaining the variability of the covariance $\boldsymbol{\Sigma}_i$ was stronger compared to that of the second component. The performance for the $p = 5$ cases (in Figure 1) is slightly better than that for the $p = 20$ cases (in Figure 2). Besides the effect of the number of subjects n on the performance, the number of time points T is also important. As the number of time points (T) increases (e.g,. $T = 40$), the estimation tends to benefit from the increased amount of information, leading to more accurate and reliable estimates of the population-level parameters as well as the subject-level parameters $u_i^{(k)}$ and the standard deviation σ of the random effects that measures the variability of the random effects $u_i^{(k)}$ across individuals.

n	T	$\gamma_1^{(1)}$	$\gamma_2^{(1)}$	$\gamma_3^{(1)}$	$\gamma_4^{(1)}$	$\gamma_5^{(1)}$	$\gamma_1^{(2)}$	$\gamma_2^{(1)}$	$\gamma_3^{(2)}$	$\gamma_4^{(2)}$	$\gamma_5^{(2)}$	$\beta_1^{(1)}$	$\beta_2^{(1)}$	$\beta_1^{(2)}$	$\beta_2^{(2)}$	σ
50	10	0.92	0.82	0.88	0.92	0.94	0.92	0.88	0.74	0.93	0.89	0.87	0.86	0.90	0.83	0.91
	20	0.91	0.85	0.88	0.94	0.89	0.95	0.83	0.82	0.87	0.92	0.93	0.89	0.90	0.85	0.94
	40	0.92	0.90	0.93	0.93	0.94	0.93	0.90	0.83	0.95	0.94	0.91	0.91	0.90	0.93	0.97
100	10	0.94	0.88	0.88	0.91	0.89	0.90	0.89	0.86	0.91	0.95	0.95	0.89	0.89	0.89	0.92
	20	0.91	0.86	0.89	0.95	0.96	0.93	0.87	0.89	0.92	0.92	0.94	0.92	0.86	0.90	0.95
	40	0.96	0.93	0.94	0.94	0.90	0.97	0.96	0.96	0.92	0.98	0.95	0.91	0.92	0.96	0.96
200	10	0.94	0.92	0.92	0.84	0.90	0.92	0.94	0.93	0.89	0.95	0.94	0.95	0.96	0.97	0.78
	20	0.93	0.94	0.96	0.94	0.92	0.95	0.94	0.97	0.91	0.92	0.96	0.95	0.95	0.94	0.93
	40	0.93	0.95	0.94	0.90	0.93	0.89	0.91	0.91	0.96	0.93	0.95	0.95	0.96	0.92	0.92
400	10	0.94	0.92	0.95	0.90	0.91	0.92	0.94	0.90	0.89	0.87	0.94	0.97	0.94	0.93	0.77
	20	0.94	0.91	0.95	0.95	0.96	0.95	0.98	0.94	0.97	0.93	0.99	0.96	0.93	0.97	0.87
	40	0.96	0.98	0.99	0.96	0.94	0.95	0.97	0.96	0.94	0.89	0.94	0.98	0.93	0.94	0.90

Table 1: The proportion of time that 95% posterior credible intervals contain the true values of the loading coefficient vectors $\gamma_j^{(k)}$ $(j = 1, \ldots, 5)$ $(k = 1, 2)$, the regression coefficients $\beta_j^{(k)}$ $(j = 1, 2)$ $(k = 1, 2)$ and σ out of 100 simulation replications, with varying $n \in \{50, 100, 200, 400\}$ and $T \in \{10, 20, 40\}$.

The results in Table 1 for the $p = 5$ cases indicate that the "actual" coverage probability is reasonably close to the "nominal" coverage probability of 0.95, especially when the sample sizes n and T are relatively large (e.g., $n = 400$, $T = 40$). The results for $p = 20$ cases were also similar. The results in Table 1 suggest that the Bayesian credible intervals exhibit reasonably good frequentist coverage, providing estimates of the parameter uncertainty that aligns with the desired coverage level, reasonably achieving nominal coverage.

4 Application

In this section, we applied the Bayesian covariate-assisted principal regression model to data from HCP. As in Seiler and Holmes [2017], we used the rs-fMRI data from 820 subjects and examined the associations between rs-fMRI and sleep duration. Each subject underwent 4 complete 15-minute sessions (with TR = 750ms, corresponding to 1200 time points per session for each subject), and each 15-minute run of each subject's rfMRI data was preprocessed according to Smith et al. [2013]. We focused on the first session which is about a typical duration for rs-fMRI studies. We also applied the method to the other three sessions to examine the sensitivity and the reliability of the modeling procedure (see Table 2). We used a data-driven parcellation based on spatial ICA with $p = 15$ components (i.e., using $p = 15$ data-driven "networks nodes"; see Figure 3 for their most relevant axial slices in MNI152 space) from the HCP PTN (Parcellation + Timeseries + Netmats) dataset, where each subject's rs-fMRI timeseries data were mapped onto the set of ICA maps [Filippini et al., 2009]; see Smith et al. [2013] for details about preprocessing and the ICA time series computation. We applied the Bayesian CAP regression to conduct statistical inference on the association between the FC over these IC networks nodes [Smith et al., 2012] and the covariates.

As in Seiler and Holmes [2017], we classified the subjects into two groups: a group of 489 conventional sleepers (average sleep duration between 7 and 9 hours each night) and a group of 241 short sleepers (average equal or less than 6 hours each night). This yielded a total of 730 participants to compare FC over the network nodes between short and conventional sleepers, adjusted for gender as an additional covariate. This type of analysis can provide insights into the

potential differences in FC between the two groups and help investigate the relationship between sleep duration and brain connectivity.

Since the time series are temporally correlated, we inferred the equivalent sample size of independent samples. We computed the effective sample size (ESS) defined by Kass et al. [1998], ESS $= \min_{i\in\{1,\ldots,n\},j\in\{1,\ldots,p\}} \left(\frac{T_i}{1+2\sum_{t=1}^{\infty} \text{cor}(Y_{i,1}^{(j)}, Y_{i,1+t}^{(j)})} \right)$, where $Y_{i,l}^{(j)}$ is the data at time l of the jth network node for subject i, following a conservative approach taking the minimum over all p components and n subjects as the overall estimator. Based on the estimated ESS, we performed thinning of the observed timeseries data, subsampling $T_i = T = \text{ESS} = 35$ time points for each subject. The resulting outcome data, $\boldsymbol{Y}_{i,l}$ $(i = 1, \ldots, n)$ $(l = 1, \ldots, T)$, were then mean-removed per each subject (so that $\sum_{i=1}^{T} \boldsymbol{Y}_{i,l} = \boldsymbol{0} \in \mathbb{R}^{15}$ for each i), and we focused on the association between the covariance $\boldsymbol{\Sigma}_i$ and covariates $\boldsymbol{x}_i$.

Using the deviation from diagonality criterion, the approach identified only a single projection component (i.e., $d = 1$), but for the purpose of illustration, here we present the results from a two-component model (i.e., $d = 2$), where the two projection components are denoted as C_1 and C_2. The model coefficients and credible intervals from the single-component model $(d = 1)$ are reported in Supplementary Materials which are numerically very close to those associated with the first component C_1 of the two-component model. In Figure 4, we summarize the marginal posterior distribution of the orthonormal loading coefficient (projection) vectors, $\boldsymbol{\gamma}^{(1)} \in \mathbb{R}^{15}$ (displayed in the upper panel) and $\boldsymbol{\gamma}^{(2)} \in \mathbb{R}^{15}$ (displayed in the lower panel) that defines the two FC components, using credible intervals Bonferroni corrected by setting the endpoints at the $0.025/p$ and $(1 - 0.025/p)$ quantiles. In Figure 5, we also display the marginal posterior distribution of the regression coefficients $\boldsymbol{\beta}^{(1)}$ and $\boldsymbol{\beta}^{(2)}$ associated with these two components (C_1 and C_2), representing the effects of the covariates on the estimated two components.

The results in Figure 5 indicate that the both FC components C_1 and C_2 are positively associated with sleep duration. See Supplementary Materials S2 for explantation on the loading coefficients interpretation. In short, being a short sleeper (compared to being a conventional sleeper) suggests a higher connectivity between two network nodes from the same color (i.e., two network nodes in the same loading sign), while suggesting a lower connectivity between two regions from different colors (i.e., two network nodes in the opposing signs), all the other components being held constant.

Specifically, in Figure 5, the model coefficients $\boldsymbol{\beta}^{(1)}$ for "Sleep duration" (short-sleeper) and for "Gender" (male) associated with the first FC component (C_1) are both positive, indicating that FC between the nodes Net9 and Net1 (cerebellum and visual area, that have the opposite loading signs) is weaker for short-sleepers, compared to conventional sleepers, holding all the other components constant. On the other hand, FC between the nodes Net9 and Net15 (cerebellum and default network, that have the same loading sign) is stronger for short-sleepers, compared to conventional sleepers, holding all the other components constant.

In Figure 5, the model coefficients $\boldsymbol{\beta}^{(2)}$ for sleep duration and gender associated with the second FC component (C_2) are also positive, as in those of C_1. Although similar covariate effects are shown for the second FC component C_2 as for the first FC component C_1, the effect magnitude for the second component C_2 is weaker than that of the first component C_1 (note that the estimated components in model (5) are rank-ordered according to the variation in the expected log-variance they explain), and the C_1 and C_2's loading coefficient vectors are orthogonal to each other. These two components with different loading coefficients provide complimentary information on the underlying FC relevant to the external covariates.

Model coefficients		Session 1	Session 2	Session 3	Session 4
C_1	Net1	0.37 (0.35, 0.39)	0.42 (0.40, 0.44)	0.38 (0.36, 0.40)	0.39 (0.37, 0.41)
	Net2	0.03 (0.01, 0.04)	0.02 (0.01, 0.04)	0.02 (0.01, 0.04)	0.02 (0.01, 0.03)
	Net3	0.32 (0.29, 0.34)	0.24 (0.21, 0.27)	0.32 (0.29, 0.34)	0.29 (0.27, 0.32)
	Net4	0.03 (0.01, 0.04)	0.06 (0.04, 0.07)	0.05 (0.03, 0.06)	0.02 (0.01, 0.04)
	Net5	0.01 (0.00, 0.03)	0.02 (0.00, 0.03)	0.02 (0.01, 0.03)	0.02 (0.01, 0.03)
	Net6	-0.02 (-0.03, -0.01)	-0.01 (-0.03, 0.00)	-0.02 (-0.03, -0.01)	-0.02 (-0.04, -0.01)
	Net7	-0.07 (-0.09, -0.06)	-0.07 (-0.08, -0.05)	-0.07 (-0.08, -0.06)	-0.08 (-0.09, -0.06)
	Net8	0.58 (0.56, 0.60)	0.51 (0.48, 0.54)	0.56 (0.54, 0.58)	0.50 (0.47, 0.52)
	Net9	-0.53 (-0.55, -0.51)	-0.57 (-0.59, -0.55)	-0.54 (-0.56, -0.53)	-0.57 (-0.58, -0.55)
	Net10	0.19 (0.17, 0.20)	0.21 (0.19, 0.22)	0.19 (0.18, 0.21)	0.21 (0.20, 0.22)
	Net11	0.21 (0.19, 0.22)	0.21 (0.19, 0.22)	0.21 (0.20, 0.23)	0.22 (0.20, 0.23)
	Net12	0.08 (0.07, 0.10)	0.12 (0.10, 0.14)	0.09 (0.08, 0.11)	0.14 (0.12, 0.15)
	Net13	0.20 (0.18, 0.22)	0.24 (0.22, 0.26)	0.20 (0.18, 0.22)	0.26 (0.24, 0.27)
	Net14	-0.01 (-0.02, 0.00)	-0.02 (-0.03, -0.01)	-0.01 (-0.02, 0.00)	-0.02 (-0.03, -0.01)
	Net15	-0.08 (-0.10, -0.07)	-0.08 (-0.10, -0.07)	-0.09 (-0.11, -0.08)	-0.11 (-0.12, -0.09)
	Sleep duration (short-sleeper)	0.35 (0.22, 0.48)	0.37 (0.23, 0.50)	0.32 (0.18, 0.45)	0.34 (0.21, 0.46)
	Gender (male)	0.19 (0.09, 0.34)	0.19 (0.08, 0.34)	0.20 (0.05, 0.31)	0.23 (0.04, 0.28)
C_2	Net1	0.22 (0.19, 0.25)	0.20 (0.17, 0.23)	0.27 (0.24, 0.30)	0.08 (0.05, 0.12)
	Net2	0.00 (-0.02, 0.02)	-0.01 (-0.03, -0.00)	-0.01 (-0.04, 0.02)	0.01 (-0.01, 0.03)
	Net3	-0.65 (-0.68, -0.63)	-0.69 (-0.72, -0.66)	-0.73 (-0.75, -0.70)	-0.50 (-0.56, -0.45)
	Net4	0.09 (0.07, 0.11)	0.08 (0.06, 0.10)	0.10 (0.07, 0.12)	-0.37 (-0.42, -0.33)
	Net5	0.05 (0.03, 0.06)	0.03 (0.0, 0.05)	0.01 (-0.01, 0.03)	-0.19 (-0.21, -0.17)
	Net6	-0.01 (-0.03, 0.00)	0.00 (-0.02, 0.01)	-0.04 (-0.06, -0.03)	-0.08 (-0.10, -0.06)
	Net7	0.01 (-0.01, 0.02)	0.02 (0.00, 0.04)	0.00 (-0.02, 0.02)	-0.04 (-0.06, -0.01)
	Net8	-0.38 (-0.40, -0.35)	-0.45 (-0.48, -0.42)	-0.33 (-0.36, -0.30)	0.60 (0.57, 0.64)
	Net9	-0.36 (-0.39, -0.33)	-0.26 (-0.30, -0.23)	-0.31 (-0.33, -0.28)	0.18 (0.14, 0.22)
	Net10	0.10 (0.08, 0.12)	0.05 (0.03, 0.08)	0.06 (0.04, 0.08)	-0.18 (-0.20, -0.16)
	Net11	0.15 (0.13, 0.17)	0.13 (0.11, 0.16)	0.17 (0.15, 0.19)	-0.01 (-0.05, 0.02)
	Net12	0.23 (0.21, 0.25)	0.22 (0.20, 0.24)	0.19 (0.17, 0.21)	-0.28 (-0.31, -0.25)
	Net13	0.37 (0.35, 0.39)	0.35 (0.33, 0.37)	0.32 (0.30, 0.35)	0.09 (0.05, 0.13)
	Net14	-0.06 (-0.07, -0.04)	-0.03 (-0.05, -0.01)	-0.06 (-0.07, -0.04)	0.13 (0.11, 0.16)
	Net15	-0.11 (-0.13, -0.09)	-0.10 (-0.12, -0.08)	-0.10 (-0.12, -0.08)	0.14 (0.11, 0.16)
	Sleep duration (short-sleeper)	0.21 (0.06, 0.32)	0.21 (0.10,0.34)	0.18 (0.07, 0.34)	0.17 (0.11, 0.35)
	Gender (male)	0.13 (-0.01, 0.25)	0.12 (0.01, 0.24)	0.13 (0.01, 0.26)	0.14 (0.02, 0.25)
σ		0.81 (0.78, 0.84)	0.81 (0.78, 0.85)	0.81 (0.78, 0.85)	0.76 (0.73, 0.79)

Table 2: The posterior medians (and 95% credible intervals) of the loading coefficients and the covariate effect coefficients of the two identified components (C_1 and C_2) and the noise standard deviations (σ) of the models, separately fitted based on the data from the 4 sessions. The results suggest that the FC associated with the sessions are relatively consistent across the 4 scanning sessions.

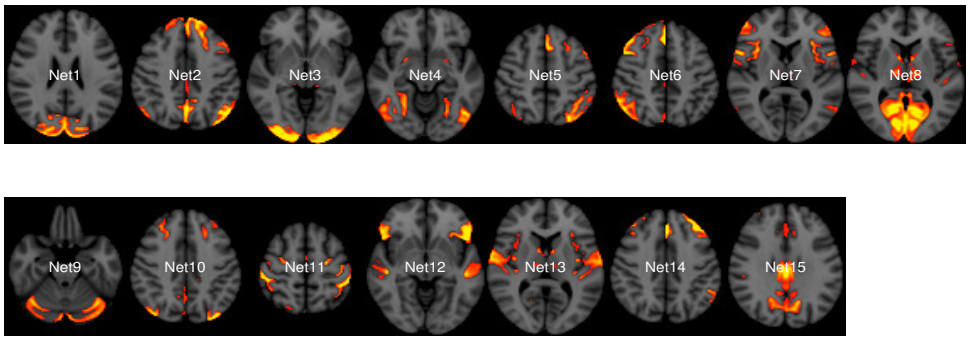

Figure 3: 15 independent components (ICs) from spatial group-ICA constituting a data-driven parcellation with 15 components ("network nodes"), provided by the HCP PTN dataset, represented at the most relevant axial slices in MNI152 space. According to Seiler and Holmes [2017], these parcels correspond to default network (Net15), cerebellum (Net9), visual areas (Net1, Net3, Net4 and Net8), cognition-language (Net2, Net5, Net10 and Net14), perception-somesthesis-pain (Net2, Net6, Net10 and Net14), sensorimotor (Net7 and Net11), executive control (Net12) and auditory (Net12 and Net13).

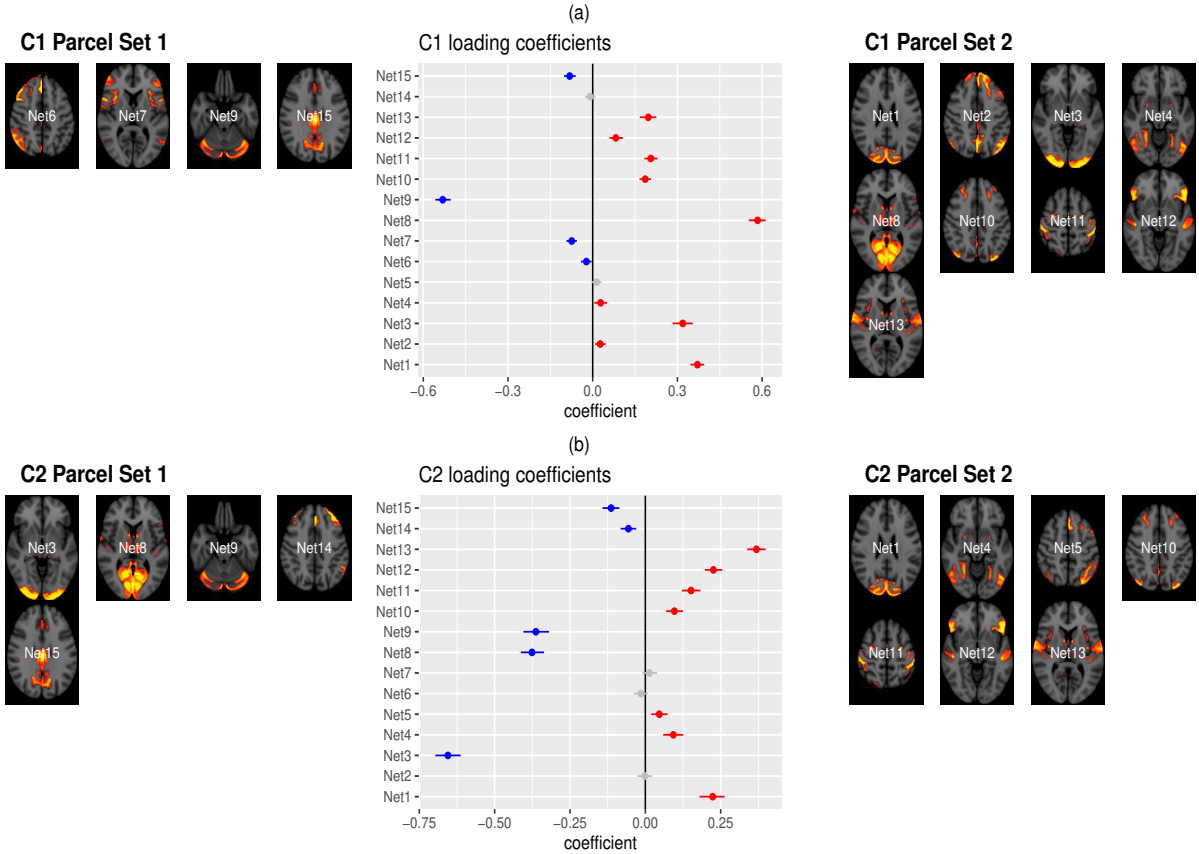

Figure 4: Credible intervals of the loading coefficients $\boldsymbol{\gamma}^{(1)}$ and $\boldsymbol{\gamma}^{(2)}$ associated with the two projection components C_1 and C_2.

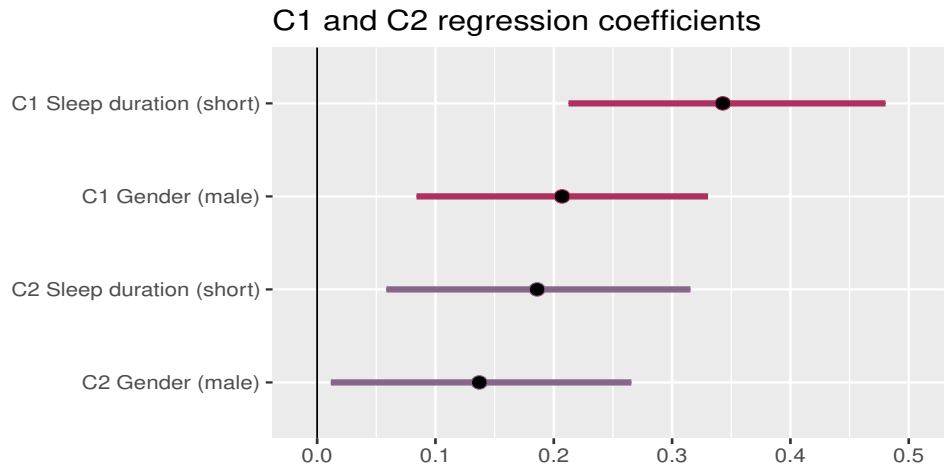

Figure 5: The posterior medians and 95% credible intervals of the regression coefficients $\boldsymbol{\beta}^{(1)}$ and $\boldsymbol{\beta}^{(2)}$ associated with the two components C_1 and C_2.

5 Discussion

Extending the frequentist approach developed in Zhao et al. [2021a], the proposed Bayesian estimation approach provides a framework to conduct inference on all model parameters simultaneously, effectively fusing dimension reduction for covariance matrices and regression model estimation in one single step. The approach allows for an inference that accounts for the uncertainties in the dimension reduction in the subsequent inference on covariate-related connectivity. In particular, the estimation does not require the computation of the full p-by-p sample covariance matrix (except for the computation of a reference point for tangent space parametrization) or modeling of the full covariance matrix. Instead, it focuses on dimension-reduced signals (as the likelihood is specified based on (5)). The CAP regression approach proposed by Zhao et al. [2021a] allows for a more targeted and efficient analysis by considering the specific components of the data that are relevant to analyzing the relationships between FC and covariates. Although, by reducing the dimensionality of the data, the computational burden and complexity associated with estimating and manipulating the full p-by-p sample covariance matrix can be significantly alleviated, the method is not suitable to be run in very high-dimensional data, such as voxel-level data. The method is generally better suited to be run in intermediate spaces, such as those produced by ICA or an anatomical parcellation. Overfitting might occur due to the large number of parameters in the estimation of the projection matrix $\boldsymbol{\Gamma}$. Future work will apply prior distributions on the dimension reducing matrix $\boldsymbol{\Gamma}$ as well as the covariate effect parameters $\boldsymbol{B}$ that promote sparsity, for parsimonious modeling with better estimability and interpretability.

In conducting the posterior inference, the assumption that we make is partially common eigenvectors of the covariance structure [Wang et al., 2021] as in Zhao et al. [2021a,b, 2022]. The covariance is decomposed into shared and unique components, where the shared component corresponds to the common eigenvectors and captures the information related to the covariates. Specifically, the approach decomposes individual covariance matrices $\boldsymbol{\Sigma}_i$ into individual-specific eigenvalues $\boldsymbol{\Lambda}_i$ and common eigenvector $\boldsymbol{\Gamma}$, while simultaneously fitting a regression model for the log of the individual-specific eigenvalues in the Bayesian paradigm. Future work may consider modeling of the heterogeneity of $\boldsymbol{\Gamma}$ with covariates. A posterior inference on $\boldsymbol{\Gamma}$ in the Stiefel manifold is introduced. A tangent space parametrization is introduced to model the variability of these PC decompositions across subjects with subject-level covariates. We also accounted for the additional subject-specific variability by including the subject-specific random intercepts. The approach provides joint inference that has shown to have good numerical properties in simulations. The tangent space parameterization introduced involves mapping the parameters onto a tangent space at a specific point on the manifold. It is often desirable to choose a reference point that is close to the observed data points in the manifold. For this reason, we used the sample marginal covariance computed across all subjects as a reference point. Selecting a reference point that is far from the data can result in a poor approximation and potential bias in the estimation as the tangent space may not adequately account for the complexity or structure of the underlying SPD manifold. Future work will involve extending this Bayesian estimation approach to the setting of analyzing dynamic FC.

Acknowledgements

Data were provided by the Human Connectome Project, WU-Minn Consortium (Principal Investigators: David Van Essen and Kamil Ugurbil; 1U54MH091657) funded by the 16 NIH Institutes and Centers that support the NIH Blueprint for Neuroscience Research; and by the McDonnell Center for Systems Neuroscience at Washington University.

References

Y. Zhao, B. Wang, S. H. Mostofsky, B.S. Caffo, and X. Luo. Covariate assisted principal regression for covariance matrix outcomes. *Biostatistics*, 22:629–645, 2021a.

Emily B. Fox and David B. Dunson. Bayesian nonparametric covariance regression. *Journal of Machine Learning Research*, 16(77):2501–2542, 2015.

M. A. Lindquist. The statistical analysis of fMRI data. *Statistical Science*, 23(4):439–464, 2008.

R. P. Monti, P. Hellyer, D. Sharp, R. Leech, C. Anagnostopoulos, and G. Montana. Estimating time-varying brain connectivity networks from functional mri time series. *Neuroimage*, 103:427–443, 2014.

A. Fornito, A. Zalesky, and M. Breakspear. Graph analysis of the human connectome: promise, progress, and pitfalls. *Neuroimage*, 15(80):426–444, 2013.

A. Fornito and E. T. Bullmore. Connectomic intermediate phenotypes for psychiatric disorders. *Frontiers in psychiatry*, 3:32, 2012.

G. Varoquaux, F. Baronnet, A. Kleinschmidt, P. Fillard, and B. Thirion. Detection of brain functional-connectivity difference in post-stroke patients using group-level covariance modeling. *Med Image Comput Comput Assist Interv*, 13:200–208, 2010.

K. J. Friston. Functional and effective connectivity: a review. *Brain Connectivity*, 1(1):13–36, 2011.

M.P. van der Heuvel and H.E. Hulshoff Pol. Exploring the brain network: a review on resting-state fMRI functional connectivity. *European Neuropsychopharmacology*, 20(8):519–534, 2010.

R.M. Hutchison, T. Womelsdorf, E.A. Allen, P.A. Bandettini, V.D. Calhoun, M. Corbetta, P.S. Della, J.H. Duyn, G.H. Glover, J. Gonzalez-Castillo, D.A. Handwerker, S. Keilholz, V. Kiviniemi, D.A. Leopold, F. de Pasquale, O. Sporns, M. Walter, and C. Chang. Dynamic functional connectivity: promise, issues, and interpretations. *Neuroimage*, 80: 360–378, 2013.

J. Whittaker. *Graphical Models in Applied Multivariate Statistics*. Wiley Series in Probability and Mathematical Statistics, John Wiley and Sons, Chichester., 1990.

M. Hinne, L. Ambrogioni, R. J. Janssen, T. Heskes, and M. A. van Gerven. Structurally-informed bayesian functional connectivity analysis. *Neuroimage*, 1(86):294–305, 2014.

J. Guo, E. Levina, G. Michailidis, and J. Zhu. Joint estimation of multiple graphical models. *Biometrika*, 98:1–15, 2011.

P. Danaher, P. Wang, and D. M. Witten. The joint graphical lasso for inverse covariance estimation across multiple classes. *Journal of the Royal Statistical Society, Series B*, 76:373–397, 2014.

Y. Xia and L. Li. Hypothesis testing of matrix graph model with application to brain connectivity analysis. *Biometrics*, 73(3):780–791, 2017.

Y. Xia, T. Cai, and T. T. Cai. Multiple testing of submatrices of a precision matrix with applications to identification of between pathway interactions. *Journal of the American Statistical Association*, 113(521):328–339, 2018.

Manjari Narayan, Genevera I. Allen, and Steffie Tomson. Two sample inference for populations of graphical models with applications to functional connectivity. *arXiv preprint arXiv:1502.03853*, 2015.

D. Durante and David B. Dunson. Bayesian inference and testing of group differences in brain networks. *Bayesian Analysis*, 13(1):29–58, 2018.

Y. Xia, T. Cai, and T. T. Cai. Testing differential networks with applications to the detection of gene-gene interactions. *Biometrika*, 102(2):247–266, 2015.

T. T. Cai, H. Li, W. Liu, and J. Xie. Joint estimation of multiple high-dimensional precision matrices. *Statistica Sinica*, 26(2):445–464, 2016.

T. Saegusa and A. Shojaie. Joint estimation of precision matrices in heterogeneous populations. *Electronic Journal of Statistics*, 10(1):1341–1392, 2016.

C. B. Peterson, F. C. Stingo, and M. Vannucci. Bayesian inference of multiple gaussian graphical models. *Journal of the American Statistical Association*, 110(509):159–174, 2015.

Linda S. L. Tan, Ajay Jasra, Maria De Iorio, and Timothy M. D. Ebbels. Bayesian inference for multiple gaussian graphical models with application to metabolic association networks. *Annals of Applied Statistics*, 11(4):2222–2251, 2017.

Z. Lin, T. Wang, C. Yang, and H. Zhao. On joint estimation of gaussian graphical models for spatial and temporal data. *Biometrics*, 73(3):769–779, 2017.

H. Liu, X. Chen, L. Wasserman, and J. Lafferty. Graph-valued regression. *Advances in Neural Information Processing Systems 23 (NIPS 2010)*, pages 1423–1431, 2010.

M. Kolar, A. P. Parikh, and E. P. Xing. On sparse nonparametric conditional covariance selection. *in ICML-10, Madison, WI: Omnipress*, pages 559–566, 2010.

K. H. Lee and L. Xue. Nonparametric finite mixture of gaussian graphical models. *Technometrics*, 60(4):511–521, 2018.

Yang Ni, C. Stingo, Francesco, and Veerabhadran Baladandayuthapani. Bayesian graphical regression. *Journal of the American Statistical Association*, 114(525):184–197, 2019.

Z. Wang, A. O. Kaseb, H. M. Amin, M. M. Hassan, W. Wang, and J. S. Morris. Bayesian edge regression in undirected graphical models to characterize interpatient heterogeneity in cancer. *Journal of the American Statistical Association*, 117(538):533–546, 2022.

J. Zhang and Y. Li. High-dimensional gaussian graphical regression models with covariates. *Journal of the American Statistical Association*, 2022.

G. G. Leday, G. B. de Gunst, M. C. Kpogbezan, A. W. van der Vaart, W. N. van Wieringen, and M. A. van de Wiel. Gene network reconstruction using global-local shrinkage priors. *Annals of Applied Statistics*, 11(1):41–68, 2017.

Nicolai Meinshausen and Peter Buhlmann. High-dimensional graphs and variable selection with the lasso. *The Annals of Statistics*, 34(3):1436–1462, 2006.

J. Peng, P. Wang, N. Zhou, and J. Zhu. Partial correlation estimation by joint sparse regression models. *Journal of the American Statistical Association*, 104(486):735–746, 2009.

J. Cheng, E. Levina, P. Wang, and J. Zhu. A sparse ising model with covariates. *Biometrics*, 70(4):943–953, 2014.

M. J. Ha, F. C. Stingo, and V. Baladandayuthapani. Bayesian structure learning in multi-layered genomic networks. *Journal of the American Statistical Association*, 116(534):605–618, 2021.

W. W. Sun and L. Li. Store: Sparse tensor response regression and neuroimaging analysis. *Journal of Machine Learning Research*, 18:1–37, 2017.

L. Li and X. Zhang. Parsimonious tensor response regression. *Journal of the American Statistical Association*, 112: 1131–1146, 2017.

E. F. Lock. Tensor-on-tensor regression. *Journal of Computational and Graphical Statistics*, 27:638–647, 2018.

M. Dai, Z. Zhang, and A. Srivastava. Analyzing dynamical brain functional connectivity as trajectories on space of covariance matrices. *in IEEE Transactions on Medical Imaging*, 39(3):611–620, 2020.

M Harandi, M. Salzmann, and R. Hartley. Dimensionality reduction on SPD manifolds: The emergence of geometry-aware methods. *IEEE Transactions on Pattern Analysis and Machine Intelligence*, 40:48–62, 2017.

Y. Li and R. Lu. Locality preserving projection on SPD matrix lie group: algorithm and analysis. *Sci. China Inf. Sci.*, 61:092104, 2018.

W. Gao, Z. Ma, C. Xiong, and T. Gao. Dimensionality reduction of SPD data based on Riemannian manifold tangent spaces and local affinity. *Applied Intelligence*, 53:1887–1911, 2023.

X. Xie, Z. L. Yu, H. Lu, Z. Gu, and Y. Li. Motor imagery classification based on bilinear sub-manifold learning of symmetric positive-definite matrices. *IEEE Trans Neural Syst Rehabil Eng.*, 25(6):504–516, 2017.

A. Davoudi, S. S. Ghidary, and K. Sadatnejad. Dimensionality reduction based on distance preservation to local mean for symmetric positive definite matrices and its application in brain–computer interfaces. *Journal of Neural Engineering*, 14(3):036019, 2017.

B. N. Flury. Common principal components in k groups. *Journal of the American Statistical Association*, 79:892–898, 1984.

B. N. Flury. Asymptotic theory for common principal component analysis. *The Annals of Statistics*, 14:418–430, 1986.

R. J. Boik. Spectral models for covariance matrices. *Biometrika*, 89:159–182, 2002.

M. Pourahmadi, M. J. Danielrs, and T. Park. Simultaneous modelling of the Cholsky decomposition of several covariance matrices. *Journal of Multivariate Analysis*, 98:568–587, 2007.

P. Hoff. A hierarchical eigenmodel for pooled covariance estimation. *Journal of the Royal Statistical Society. Series B (Statistical Methodology)*, 71(5):971–992, 2009.

A. M. Franks and P. Hoff. Shared subspace models for multi-group covariance estimation. *Journal of Machine Learning Research*, pages 1–37, 2019.

B. Li and E. Solea. A nonparametric graphical model for functional data with application to brain networks based on fmri. *Journal of the American Statistical Association*, 113(524):1637–1655, 2018.

J. Zhang, Sun W. Wei, and L. Li. Mixed-effect time-varying network model and application in brain connectivity analysis. *Journal of the American Statistical Association*, 115(532):2022–2036, 2020.

P. Hoff and X. Niu. A covariance regression model. *Statistica Sinica*, 22:729–753, 2012.

Tao Zou, Wei Lan, Hansheng Wang, and Chih-Ling Tsai. Covariance regression analysis. *Journal of the American Statistical Association*, 112:266–281, 2017.

Mohsen Pourahmadi. Covariance estimation: The GLM and regularization perspectives. *Statistical Science*, 26(3): 369–387, 2011.

Y. Zhao, B.S. Caffo, and X. Luo. Principal regression for high dimensional covariance matrices. *Electronic Journal of Statistics*, 15:4192–4235, 2021b.

Y. Zhao, B.S. Caffo, and X. Luo. Longitudinal regression of covariance matrix outcomes. *Biostatistics*, page kxac045, 2022.

R. F. Engle and K. F. Kroner. Multivariate simultaneous generalized ARCH. *Econometric Theory*, 11:122–150, 1995.

P. W. Fong, W. K. Li, and H. Z. An. A simple multivariate ARCH model specified by random coefficients. *Computational Statistics and Data Analysis*, 51:1779–1802, 2006.

S. B. Eickhoff, B. T. T. Yeo, and S. Genon. Imaging-based parcellations of the human brain. *Nat Rev Neurosci.*, 19(11): 672–686, 2018.

S. M. Smith, K. L. Miller, S. Moeller, J. Xu, E. J Auerbach, M. W. Woolrich, C. F. Beckmann, M. Jenkinson, J. Andersson, M. F. Glasser, D. C. Van Essen, D. A. Feinberg, E. S. Yacoub, and K. Ugurbil. Temporally-independent functional modes of spontaneous brain activity. *Proc Natl Acad Sci U S A*, 109(8):3131–3136, 2012.

Vince D. Calhoun, Jingyu Liu, and Tulay Adali. A review of group ica for fmri data and ica for joint inference of imaging, genetic, and erp data. *Neuroimage*, 45(1):S163–S172, 2009.

S. M. Smith, D. Vidaurre, C. F. Beckmann, M. F. Glasser, M. Jenkinson, K. L. Miller, T. E. Nichols, E. C. Robinson, G. Salimi-Khorshidi, M. W. Woolrich, D. M. Barch, K. Ugurbil, and D. C. Van Essen. Functional connectomics from resting-state fmri. *Trends in Cognitive Science*, 17(12):666–682, 2013.

D. C. Van Essen, S. M. Smith, D. M. Barch, T. E. Behrens, E. Yacoub, K. Ugurbil, and et al. The WU-Minn human connectome project: an overview. *Neuroimage*, 80:62–79, 2013.

C. Seiler and S. Holmes. Multivariate heteroscedasticity models for functional brain connectivity. *Frontiers in Neuroscience*, 11:696, 2017.

M. L. Grillon, C. Oppenheim, G. Varoquaux, F. Charbonneau, A. D. Devauchelle, M. O. Krebs, F. Bayle, B. Thirion, and C. Huron. Hyperfrontality and hypoconnectivity during refreshing in schizophrenia. *Psychiatry Research*, 211 (3):226–233, 2013.

N. D. Woodward, B. Rogers, and S. Heckers. Functional resting-state networks are differentially affected in schizophrenia. *Schizophrenia Research*, 130:86–93, 2011.

A. Schwartzman. Lognormal distributions and geometric averages of symmetric positive definite matrices. *International Statistical Review*, 84(3):456–486, 2016.

X. Pennec, P. Fillard, and N. Ayache. A Riemannian framework for tensor computing. *International Journal of Computer Vision*, 66(1):41–66, 2006.

U. Pervaiz, D. Vidaurre, M. W. Woolrich, and S. M. Smith. Optimising network modelling methods for fmri. *Neuroimage*, 211:116604, 2020.

Kisung. You and Hae-Jeong Park. Re-visiting riemannian geometry of symmetric positive definite matrices for the analysis of functional connectivity. *Neuroimage*, 225:117464, 2021.

B. Ng, G. Varoquaux, J.B. Poline, M. Greicius, and B. Thirion. Transport on riemannian manifold for connectivity-based brain decoding. *IEEE Trans. Med. Imag.*, 35(1):208–216, 2016.

Y. Chikuse. The matrix angular central gaussian distribution. *Journal of Multivariate Analysis*, 33(2):265–274, 1990.

Peter E. Jupp and Kanti V. Mardia. *Directional Statistics*. John Wiley & Sons, Incorporated, 1999.

Michael Jauch, Peter D. Hoff, and David B. Dunson. Monte Carlo simulation on the Stiefel manifold via polar expansion. *Journal of Computational and Graphical Statistics*, 30(3):622–631, 2021.

Nicholas J. Higham. Computing the polar decomposition—with applications. *SIAM Journal on Scientific and Statistical Computing*, 7(4):1059–1417, 1986.

R.M. Neal. *MCMC Using Hamiltonian Dynamics*. Chapter 5, Bocan Raton: Chapman and Hall-CRC Press, 2011.

Stan Development Team. Stan modeling language users guide and reference manual. 2023.

B. Flury and W. Gautschi. An algorithm for simultaneous orthogonal transformation of several positive definite symmetric matrices to nearly diagonal form. *SIAM Journal on Scientific and Statistical Computing*, 7:169–184, 1986.

N. Filippini, B. J. MacIntosh, M. G. Hough, G. M. Goodwin, G. B. Frisoni, S. M. Smith, P. M. Matthews, C. F. Beckmann, and C. E. Mackay. Distinct patterns of brain activity in young carriers of the apoe-e4 allele. *Proceedings of the National Academy of Sciences*, 106(17):7209–7214, 2009.

R. E. Kass, B. P. Carlin, A. Gelman, and R. Neal. Markov chain monte carlo in practice: A roundtable discussion. *The American Statistician*, 52:93–100, 1998.

B. Wang, X. Luo, Y. Zhao, and B. Caffo. Semiparametric partial common principal component analysis for covariance matrices. *Biometrics*, 77(4):1175–1186, 2021.

Supplementary Materials

S1. Performance of the "deviation from diagonality" criterion in determination of the number of components

Here we report the results from a simulated example to demonstrate the performance of the "deviation from diagonality" (DfD) criterion defined in (13). We used the same simulation scenarios as in Section 3.1. The data were generated following the simulation scenarios in Section 3.1 with varying $n \in \{50, 100, 200, 400\}$, $T_i \in \{10, 20, 40\}$, and $p \in \{5, 20\}$ with $d = 2$ number of components. For each scenario, we ran 100 simulation replications and then reported the proportion (computed across the 100 runs) that the estimated number of components is the same as the truth (i.e., $d = 2$). For each simulation run, we computed the posterior mean of DfD (13) based on the posterior MCMC samples on $\mathbf{\Gamma}$, and used the cutoff value of 1.5 to determine the number of components. In Figure S1, we display the proportions of identifying the correct number of components. For both $p = 5$ and 20, as both n and T increases, the proportion of identifying the correct number of components approximately converges to 1, suggesting that the reasonableness of the metric (13) in choosing the number of components. When $p = 20$ and the number of time points (within-subject data points) T is small ($T = 10$), the performance is less robust compared to that with a larger T ($T = 20$ or 40), as the DfD criterion is computed based on the $p \times p$ sample covariance matrix whose estimation is less reliable with smaller sample sizes.

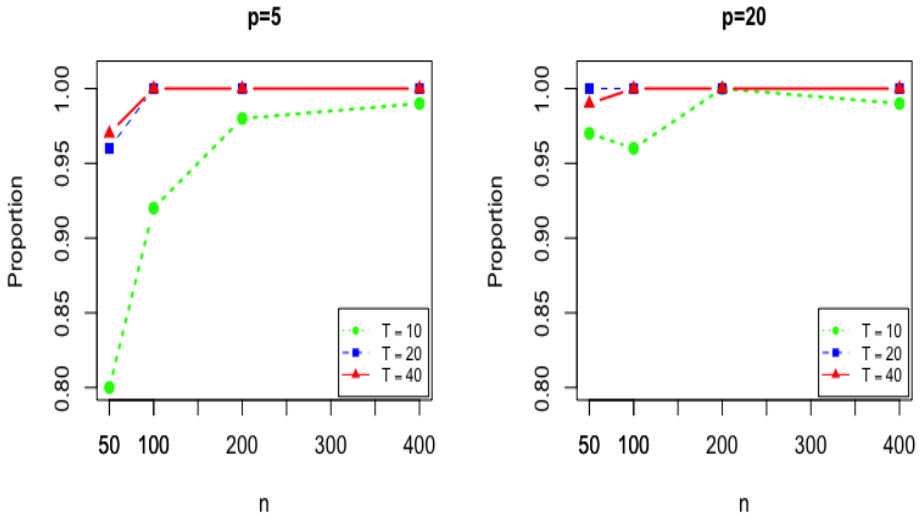

Figure S1: The proportion of identifying the correct number of components, for different simulation scenarios with $n \in \{50, 100, 200, 400\}$, $T_i \in \{10, 20, 40\}$, and $p \in \{5, 20\}$.

S2. Interpretation of the projection loading coefficients

For subject i with subject-specific pairwise correlation matrix $\mathbf{\Sigma}_i = [\sigma_{jj',i}] \in \text{Sym}_p^+$, the log-variance of the (kth) component is

$$\log\left(\boldsymbol{\gamma}^{(k)\top}\mathbf{\Sigma}_i\boldsymbol{\gamma}^{(k)}\right) = \log\left(1 + \sum_{j\neq j'}^{p} \gamma_j^{(k)}\gamma_{j'}^{(k)}\sigma_{jj',i}\right) = \beta_0^{(k)} + x_i\beta_1^{(k)} + u_i^{(k)}$$

where the kth loading direction $\boldsymbol{\gamma}^{(k)} = (\gamma_1^{(k)}, \ldots, \gamma_j^{(k)}, \ldots, \gamma_{j'}^{(k)}, \ldots, \gamma_p^{(k)})^\top \in \mathbb{R}^p$ (subject to $\|\boldsymbol{\gamma}^{(k)}\| = 1$). The model indicates that for any region pair (j, j'), the signs of the corresponding product $\gamma_j^{(k)}\gamma_{j'}^{(k)}$ and of the regression coefficient $\beta_1^{(k)}$ determine the direction of association between the pairwise correlation ($\sigma_{jj',i}$) and the covariate x_i. Here, for the simplicity in illustrating the model, $\mathbf{\Sigma}_i$ is assumed to be a correlation matrix. However, the same interpretation in terms of the direction of the association is applied to a covariance matrix $\mathbf{\Sigma}_i$.

First let us consider the case $\beta_1^{(k)} > 0$; if two brain regions (j and j') have the same loading signs, the model suggests a positive association between the correlation $\sigma_{jj',i}$ and the covariate x_i, holding all the other components constant; if the brain regions have opposite loading signs, the model suggests a negative association between the correlation $\sigma_{jj',i}$ and the covariate x_i, holding all the other components constant.

Now let us consider the case $\beta_1^{(k)} < 0$; if two brain regions (j and j') have the same loading signs, the model suggests a negative association between the correlation $\sigma_{jj',i}$ and the covariate x_i, holding all the other components constant; if the brain regions have opposite loading signs, the model suggests a positive association between the correlation $\sigma_{jj',i}$ and the covariate x_i, holding all the other components constant.

S3. The estimated model coefficients from a single-component model

The model coefficients and credible intervals from the single-component model ($d = 1$), estimated on the first session of the HCP dataset used in the Application section of the main manuscript, are displayed in Figure S2. The resulting model coefficients and posterior distributions are numerically very close to those associated with the first component C_1 of the two-component model, described in Figure 4 of the main manuscript. In Table S1, we report the posterior medians (and 95% credible intervals) of the projection loading coefficients, the covariate effect coefficients and the noise standard deviations (σ) of the single-component ($d = 1$) models, separately fitted based on the data from the 4 sessions of the HCP dataset used in the Application section of the main manuscript. The results indicate that the FC associated with the sessions are relatively consistent across the scanning sessions, and also the estimated model parameters are numerically very close to those associated with the first component C_1 of the two-component models, except for the log-variance noise standard deviation σ.

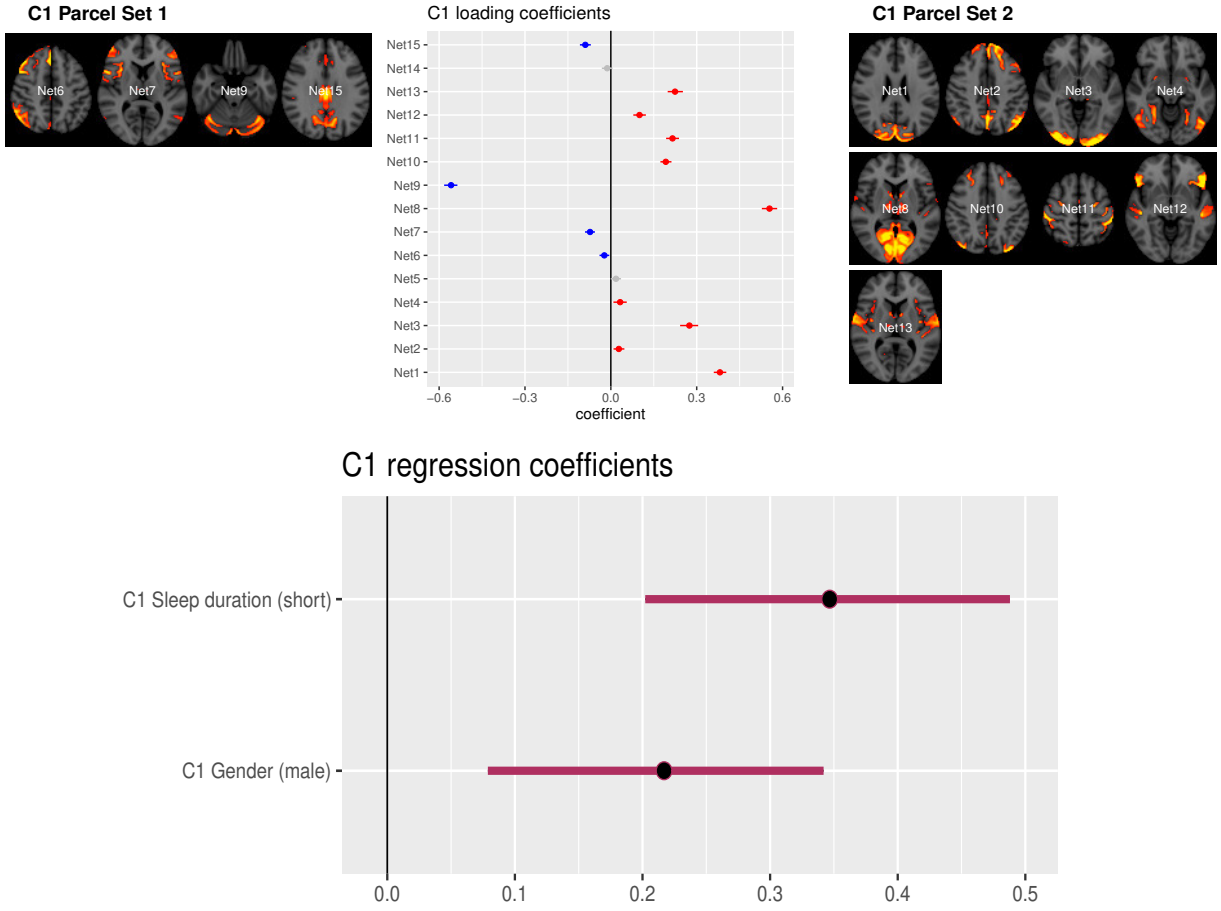

Figure S2: Credible intervals of the loading coefficients $\boldsymbol{\gamma}^{(1)}$ (upper panel) and the regression coefficients $\boldsymbol{\beta}^{(1)}$ (lower panel) of the estimated component from the single-component model.

Model coefficients		Session 1	Session 2	Session 3	Session 4
C_1	Net1	0.38 (0.37, 0.40)	0.42 (0.41, 0.44)	0.40 (0.38, 0.41)	0.39 (0.38, 0.41)
	Net2	0.03 (0.02, 0.04)	0.02 (0.01, 0.04)	0.00 (-0.01, 0.01)	0.02 (0.01, 0.04)
	Net3	0.27 (0.25, 0.30)	0.22 (0.19, 0.24)	0.28 (0.26, 0.31)	0.27 (0.24, 0.29)
	Net4	0.03 (0.02, 0.05)	0.06 (0.04, 0.08)	0.03 (0.02, 0.05)	0.01 (-0.01, 0.02)
	Net5	0.02 (0.01, 0.03)	0.02 (0.01, 0.03)	0.02 (0.00, 0.03)	0.01 (0.00, 0.02)
	Net6	-0.02 (-0.03, -0.01)	-0.01 (-0.03, 0.00)	-0.03 (-0.04, -0.02)	-0.03 (-0.04, -0.01)
	Net7	-0.07 (-0.08, -0.06)	-0.07 (-0.08, -0.05)	-0.09 (-0.10, -0.08)	-0.08 (-0.09, -0.07)
	Net8	0.55 (0.54, 0.57)	0.49 (0.47, 0.51)	0.54 (0.52, 0.56)	0.53 (0.51, 0.55)
	Net9	-0.56 (-0.57, -0.54)	-0.59 (-0.60, -0.57)	-0.55 (-0.56, -0.54)	-0.56 (-0.57, -0.54)
	Net10	0.19 (0.18, 0.21)	0.21 (0.20, 0.22)	0.21 (0.19, 0.22)	0.20 (0.19, 0.21)
	Net11	0.22 (0.20, 0.23)	0.21 (0.20, 0.23)	0.21 (0.20, 0.23)	0.22 (0.20, 0.23)
	Net12	0.10 (0.09, 0.11)	0.13 (0.12, 0.15)	0.11 (0.10, 0.13)	0.12 (0.11, 0.14)
	Net13	0.22 (0.21, 0.24)	0.25 (0.24, 0.27)	0.22 (0.20, 0.23)	0.26 (0.24, 0.28)
	Net14	-0.01 (-0.02, 0.00)	-0.02 (-0.03, -0.01)	-0.02 (-0.03, -0.01)	-0.01 (-0.03, -0.00)
	Net15	-0.09 (-0.10, -0.08)	-0.09 (-0.10, -0.07)	-0.10 (-0.12, -0.09)	-0.10 (-0.11 -0.09)
	Sleep duration (short-sleeper)	0.35 (0.22, 0.51)	0.37 (0.25, 0.53)	0.39 (0.19 0.48)	0.33 (0.21, 0.46)
	Gender (male)	0.22 (0.08 0.34)	0.21 (0.07,0.34)	0.17 (0.04 0.31)	0.17 (0.03, 0.31)
σ		0.90 (0.85 0.95)	0.90 (0.85,0.96)	0.91 (0.86 0.96)	0.90 (0.85, 0.96)

Table S1: The posterior medians (and 95% credible intervals) of the projection loading coefficients, the covariate effect coefficients and the noise standard deviations (σ) of the single-component ($d = 1$) models, separately fitted based on the data from the 4 sessions. The results suggest that the FC associated with the sessions are relatively consistent across the scanning sessions, and also the estimated model parameters are numerically very close to those associated with the first component C_1 of the two-component models, except for the log-variance noise standard deviation σ.